UNIVERSITY OF GHANA

SCHOOL OF PHYSICAL AND MATHEMATICAL SCIENCES

DEPARTMENT OF CHEMISTRY

SYNTHESIS AND CHARACTERIZATION OF AZO DYES AS SENSITIZERS FOR POSSIBLE APPLICATION IN DYE-SENSITIZED SOLAR CELLS (DSSCS)

BY

BRUCE OFFEI KWAKU ESSAH

[10279461]

THIS THESIS IS SUBMITTED TO THE UNIVERSITY OF GHANA, LEGON IN PARTIAL FULFILLMENT OF THE REQUIREMENT FOR THE AWARD OF MASTER OF PHILOSOPHY IN CHEMISTRY DEGREE

SEPTEMBER 2021

DECLARATION

I, Bruce Offei Kwaku Essah declare that the work described herein was done by me in the laboratories of the Department of Chemistry and the Department of Material Science and Engineering, University of Ghana, Legon, under supervision and has neither been presented for a degree in this University nor any other University elsewhere for another degree.

Sign:  Date: 09/ 06/ 2022

Bruce Offei Kwaku Essah

[Student]

Sign: 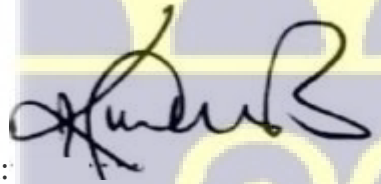 Date: 09/ 06/ 2022

Prof. Robert Kingsford-Adaboh

[Supervisor, Department of Chemistry]

Sign: 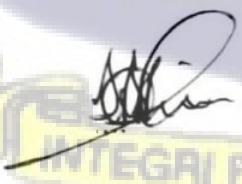 Date: 09/ 06/ 2022

Prof. David Dodoo-Arhin

[Co-supervisor, Department of Material Science Engineering]

ABSTRACT

Eight azo dyes were synthesized, purified and characterized. The Stuart Melting Point Apparatus was used to measure the melting point of the dyes, UV-Vis spectroscopy was used to measure the absorbance in the UV-Vis region, FT-IR Spectroscopy was used to determine the chemical bonds and composition of the azo dyes. The ^{1}H NMR and ^{13}C NMR were used to successfully elucidate the chemical structures of the synthesized azo dyes (DYE 1, DYE 2, DYE 3, DYE 4, DYE 5, DYE 6, DYE 7 and DYE 8). The Cyclic voltammetry was used to characterize the electrochemical behaviour of the azo dyes as sensitizers for application in Dye Sensitized Solar Cells (DSSCs). The results of the instrumentational analysis of each synthesized azo dye were compared to that of the industrial standard, inorganic ruthenizer 535-bisTBA (**N719**) dye. The photochemical optical band gap (Eg) calculated for the azo dyes ranged from 1.969 eV to 2.886 eV. The dye sensitizers showed an extrapolated electrochemical oxidation potential were between 0.28 eV to 0.66 eV with DYE 1 and DYE 8 offering the most efficient potential difference to remove an electron from their molecular orbitals. The optical band gaps of the dyes were between 1.969 eV and 2.886 eV as compared to literature value of 1.91 eV of the standard N719 dye. The low E_g of DYE 1, DYE 2, DYE 6 and DYE 7 suggest that the distances between their HOMO and LUMO levels is such that the energy in the visible region is enough to cause electron promotion from their valence band into their conduction bands. The calculated LUMO values obtained were -3.149 eV, -3.204 eV, -3.43 eV for DYE 6, DYE 7 and the standard N719 dye respectively. The DYE 3 has the highest LUMO energy level of -2.313 eV. The difference in the LUMO and the HOMO indicates that the electrochemical band gap of the standard N719 dye is 1.909 eV, which is the least followed by 1.97eV band gap energy for DYE 1. The electrochemical band gap of DYE 7 and DYE 6 were 2.81 eV and 2.28 eV respectively which were the second and third least energy values. These values were closer to that of the standard N719 dye. Out of the eight azo dyes studied, the DYE 1, DYE 6 and DYE 7 showed the best DSSCs sensitizer abilities although they were still less than that of the industrial dye.

DEDICATION

This work is dedicated to God Almighty, to the Essah Offei family and to all individuals, researchers and organizations working tirelessly to realize the Goal 7 of the Sustainable Development Goals (SDGs) which state that people should get access to reliable, affordable, sustainable and modern energy globally by 2030.

ACKNOWLEDGEMENT

I thank God Almighty for a successful completion of the MPhil. education.

My most profound gratitude goes to my supervisors, Prof. Robert Kingsford-Adaboh and Prof. David Dodoo-Arhin for their immense contributions and constructive criticisms throughout this project. This work could not have materialized, if not for your patience, time and supervision. To Mr. Jaato Bright Nsolebna, I say a big thank you for reading through my work.

A deep appreciation goes to the technical staff of the Department of Chemistry, University of Ghana, especially Mr. Samuel Owusu Atuah and David Bakomnaah for their assistance throughout the period of this project.

Finally, to my parents, Mr and Mrs Essah Offei and my dear wife, Mrs. Kate O. Essah for their love, prayers, encouragement and financial support during the high and low of the MPhil education.

TABLE OF CONTENT

LIST OF FIGURES

LIST OF TABLES

LIST OF ABBREVIATIONS

CH_3CN	Acetonitrile
CE	Counter electrode
CV	Cyclic voltammetry
DCM	Dichloromethane
DSSC	Dye sensitized solar cell
Eg	Energy
FTO	Fluorine-doped tin oxide
HOMO	Highest occupied molecular orbital
IPCE	Incident photon to current conversion efficiency
LUMO	Lowest unoccupied molecular orbital
m.p	Melting point
mL	Mililitres
Voc	Open circuit photovoltage
RT	Room Temperature
Jsc	Short circuit current density
η	Solar energy to electricity conversion efficiency
UV	Ultraviolet
WAPP	West African Power Pool

CHAPTER ONE

1.0 Introduction

1.1 Azo dyes

The role of dyes in human history since antique has been of great importance. Most traditional cultures and civilisations value the dyeing industry. Dyes are employed in commercial and industrial products for example in food, fabrics, pigments, furniture, ink, cosmetics and paints, etc. Azo dyes are a class of dyes that are used all over the world due to their diverse applications in many areas such as colouring of fabric or cloth, colouring of plastics, medicine and food colour. W. H. Perkin discovered Mauveine A in 1856, the first synthetic organic dye (Rippon & Evans, 2012). After this discovery was made, thousands of synthetic dyes have been prepared (Filarowski, 2010). Figure 1.1 illustrates the structural formula of Mauveine A.

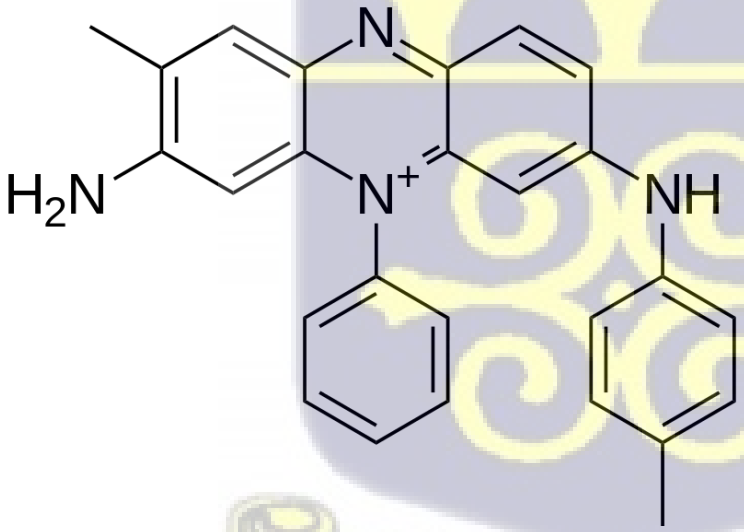

Figure 1.1: Structural formula of Mauveine A

The emergence of modern organic chemistry in 1858 resulted in the discovery of diazo compounds. Aromatic diazo compounds were discovered by Peter Griess (Lindsay, 1979). When

aromatic compounds were being studied, the concept of carbon having tetravalency was one of the new ideas. For organic chemists to obtain the details of the chemical structures of the compounds of natural products or synthetic compounds, elementary analysis was employed. Griess as cited in Yates and Yates (2016) synthesized new compounds and gave the name 'diazo', because initially he believed that benzene has two hydrogen atoms which can be substituted with the two nitrogen atoms to form salts of the type C_6H_4-N_2-HX. Further research showed that these diazo compounds were bases (Zollinger, 1994). Over 60 % of the dyes that are employed in industrial work are azo dyes. Azo dyes have recognised structure with Ar-N=N-Ar^1, where Ar and Ar^1 are two aromatic groups or akyl groups.

1.2 Global Energy Demand

Global energy demand is on the rise and the impact this has on the global economy and the environment continues to be an important topic of discussion. The fastest growing source of energy in the world today is the renewable energy. This is growing at an average rate of 2.6% per year (IEO, 2016). This tremendous growth rate is due to policies made by governments and the incentives encouraging the use of non-fossil energy sources in many countries (IEO, 2016). A Report by the International Energy Agency(IEA) shows that there was 2% reduction in world electricity demand in 2020 because of the Covid-19 pandemic (IEA, 2020). In 2021, the world economy begun to recover and electricity demand is forecasted to rise by 3%. The recovery rate would be significantly lower than the 7% which is as a result of rebound in demand in 2010, the year following the global financial crisis. China is the only country that saw a major increase in electricity demand in 2020 (IEA, 2020). Although, the estimated growth is by 2%, this growth is below its recent average of 6.5%. United States, Europe, India, Korea, Japan and Southeast Asia who are the big electricity consumers are estimated to experience reduction in electricity demand

for the year(IEA, 2020). Further report by International Energy Agency indicates that electricity generation from renewable energy – such as wind, solar and hydropower – is forecasted to grow by almost 7% in 2020, squeezing conventional power sources. According to Dr Fatih Birol, who is the IEA's Executive Director, it is estimated that the world energy today is centralized on the great role of electricity. This role will only grow high in importance as clean energy goes up. Figure 1.2 shows the statistical review of the world energy.

Figure 1.2 British Petroleum Statistical Review of World Energy (2017)

According to the IEA report, the estimated net product worldwide of energy production will increase by 3% in 2021 for coal-fired generation, while there will be 1% increment for gas-fired plants. The emission of greenhouse gases from these source will push for a global increase 2% of carbon dioxide gas in 2021 from the energy production sectors (IEA, 2020).

1.3 Energy Demand In Africa

Deriving a reliable and secure energy source is a basic driver of economic growth. Africa has diverse sources of energy, which include fossil fuels and renewable energy. Accessing affordable, reliable, sustainable and modern energy for all has been stated in the Goal 7 of the United Nations Sustainable Development Goals (SDGS) (UN General Assembly, 2015). Azo compounds are one of the largest manufactured synthetic organic compounds. Azo dyes are xenobiotic compounds and have electron withdrawing groups that create electron deficiency thereby making them resistant to degradation (Singh et al., 2014). Azo compounds are used as cathodic decolourizers in biofuel for electricity generation (Kumar et al, 2019). The beginning of work on different kinds of synthetic dyes which includes azo dyes brought the development of aluminium sheet, leather, paper, ink-jet printer and electro-optical devices (Grisafe et al., 2010). Energy is an indispensable commodity for economic growth and environmental sustainability. Access to electricity in the West African region vary from below 20% in countries like Sierra Leone, Burkina Faso, Liberia, and Niger to 50 % and more in Senegal and more than 70% in Ghana (UNESCO Science report, 2015). The total installed energy source capacity in the world is estimated to rise from 183 GW in the year 2015 to 596 GW in the year 2040 and 1835 GW in 2065 (Pappis et al, 2019). Nonetheless, the mounted electricity capacity in Africa was almost 165 GW in 2015, comparably less to the systems of China (1,519 GW) (Central Intelligence Agency, 2018), India (308 GW), and (Europe 1,030 GW) 3 (ENTSO-E, 2015)

Most of the West, East and Central African countries are ranked amongst undeveloped economies in today's world. A lot of the African countries do not have electrical power and other forms of current energy facilities, whereas those countries having accessibility have recurrent fluctuations. About two-thirds of the world's populace, roughly 600 million people found in Sub-

Saharan Africa did not have access to electricity in 2016, also 850 million people had no access to clean cooking facilities such as liquefied petroleum gas (LPG), natural gas, improved biomass cook(ICS) stoves or electricity and biogas (International Energy Agency, 2017). According to Kambiré et al (2016), people who have unstable supply of electricity have challenges in accessing portable source of water. In Ghana and Africa as a continent, there are major gaps in knowledge and data regarding the use of organic and inorganic materials as solar cells to trap the sun's energy to produce electricity for private and industrial usage. Renewable energy sources and hybrid power generating systems have become the new paradigm shift in this modern era. In the production of electricity, using renewable forms like photovoltaics materials and dye sensitized solar cells can be used. Other renewable energy sources like tidal, geothermal, wind power and hydroelectric power can be used to produce electricity. Both combined and stand-alone renewable energy technologies do not bear huge cost on fuel usage hence no reliance on consistent provision of fuels.

1.4 West Africa Power Demand and Future Scenario

West Africa continue to be in dire need of power. Other unexploited power resources in the West African region may help to reduce the challenge of power supply. Electricity is the main source of energy for many industries and houses in West Africa. Figure 1.3 below shows the total mounted energy capability installed. The west African power pool has been estimated to rise to nearly 23 times from 20 GW in 2015 to 455 GW in 2016(West African Power Pool report, 2016)

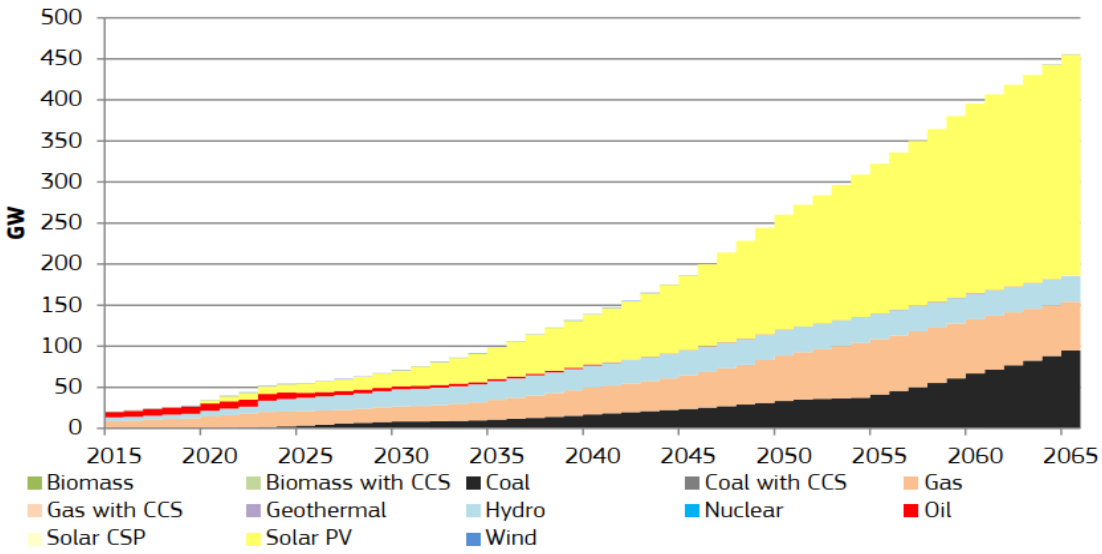

Figure 1.3 Power generation capacity Reference scenario in West African Power Pool (2019)

Figure 1.3 gives the 2.0ºC scenario which shows that by 2065 there will be investments in the future primarily in energy technologies such as biomass (8.8 GW), wind (29 GW) and solar CSP (15 GW) power plants. The number of African countries that have been highlighted to attain the yearly emission restrictions in 2.0ºC scenario. It is seen that by 2065, renewable energy will increase by 5% (71% in total of the renewable energy) compared to the reference scenario (Pappis et al, 2019).

1.5 Solar Energy Production

Solar energy is a major renewable source of energy and the most abundant energy source available to the world. The sun's solar energy can be converted into two typical applications, thermal and electrical energy. Production of solar energy can be described as the basis where the energy economy becomes viable. Solar energy is mainly used as a source of heat in many applications

such as household hot water systems, power for refrigerators, crops drying, air conditioners in homes and the operation of photovoltaic cells in for production for electricity.

1.6 Photovoltaic (PV) power Generation and Dye-sensitized solar cells

Photovoltaic cell is an electrical device in which its properties are resistance, voltage and current. When exposed to light energy, it absorbs solar energy and brings about differences in electrical properties. It portrays the processes of photoelectric cell. Photovoltaic cell or solar cell is an electrical gadget which converts the light energy from the sun straight into the production of electricity by a physico-chemical phenomenon called the photovoltaic effect. Photovoltaic devices can be made by combining single solar cell to produce what is popularly called solar panels. The solar panels with single junction silicon is the most common panel that can produce an outmost open-circuit voltage of approximately 0.5 to 0.6 volts. Photovoltaic cells have the ability to capture the sun's energy and convert into electrical energy. This is due to a photovoltaic effect created on the photovoltaic plate. The Photovoltaic effect is the principle that underlines the conversion of light to electricity in solar cells. Figure 1.4 shows an image of a solar energy system connected to a bulb. The anti-reflective coating prevents the sun's rays from being reflected. The front contact absorbs energy and the energy is carried by the semi-conductor molecules (sensitizers).The energy is further transmitted to the back contact on to a load (bulb).

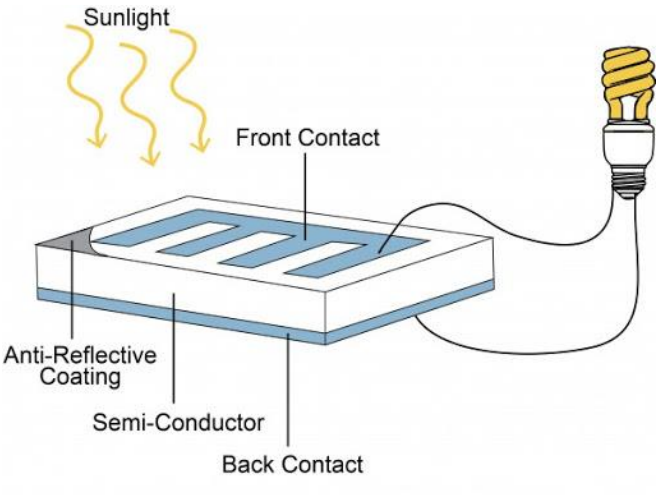

Figure 1.4 Image of a photovoltaic solar energy system connected to a bulb (Bhatia, 2014)

There are diverse photovoltaic technologies and types of the installed systems. These days, the photovoltaic modules widely in the monocrystalline silicon solar cells, microcrystalline silicon solar cells, polycrystalline silicon (or multicrystalline) solar cells, as well as the cadmium telluride and copper-indium-gallium-diselenide (CIGS) solar cells. Other solar cells are amorphous, multi-junctions, cadmium telluride cells and copper-indium-diselenide (CIS) cells, plus a gallium indium alloy. This solar energy system can provide clean power for all types of use, be they large or small. When installed, solar cells can generate energy on commercial buildings, offices, residential homes and public buildings.

There are seven main types of solar cell technologies (Sharma et al, 2021). The first generation comprises cells that are quite expensive to fabricated, and possess a low power conversion efficiency. Figure 1.5 shows diagram of dye sensitized solar cell.

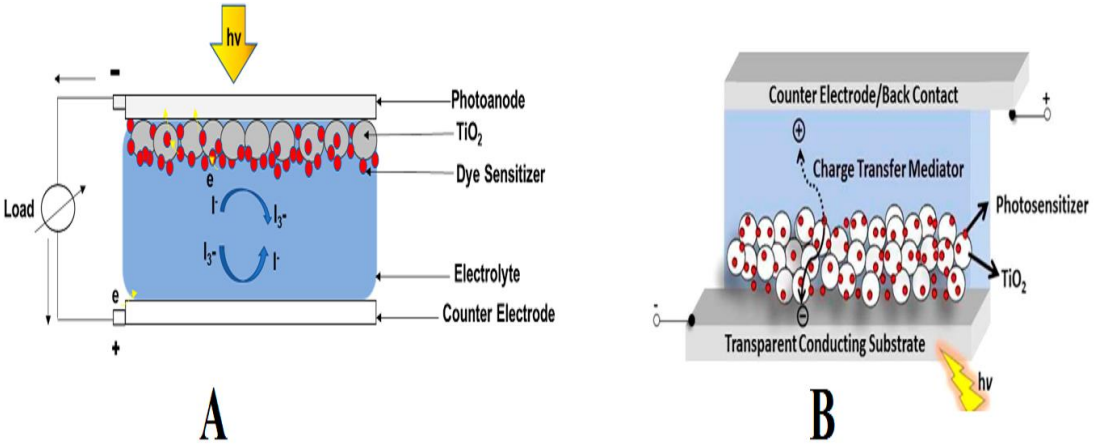

Figure 1.5 A dye-sensitized solar cell (DSSC)

Dye-sensitized solar cell (DSSC) is a device that changes light energy from the sun into electrical energy using sensitizer dye molecules coupled with semiconductor (Titanium dioxide) electrode. In the operation of dye-sensitized solar cell (DSSC), the solar energy absorbed by the dyes (sensitizers) are converted intro electrical energy, this mimics the natural process of photosynthesis, but in variance with conventional photovoltaic plates. The process is activated through photo-induced electron transfer from the excited sensitizers to a mesoporous wide-bandgap semiconductor which is usually made of Titanium (IV) oxide (TiO_2) (Banin *et al*, 2021). Earlier works indicated that in DSSC, the effect of dye sensitizers on the performance of ZnO nanorods semiconductor yielded good results. Experimental results showed that the synthetic dye achieved a higher efficiency than the natural dyes (Suyitno et al, 2015).

1.7 Problem Statement

Countries in Africa such as Ghana need to enhance access to electrical energy in order to improve the living standards of its people. According to International Energy Agency (IEA, 2016) Ghana increased access to electricity from 61% in 2010 to 84% in 2016 .The country continues to struggle with load shedding and power outages. Exploitation of the high solar potential in countries such

as, Ivory Coast, Nigeria and Ghana is somewhat low compared to other African regions (IRENA, 2018). In 2015, Ghana experienced power outages when its major source of electricity (Hydroelectric power) could not meet the 1,580MW usual demand of Ghanaians (IHA, 2015). In the past decade, Ghana has experienced severe electricity supply challenges costing the nation an average of US $2.1 million in buying power for production daily (Nyarko-Kumi, 2017). The dependence on petroleum products by households to power generators to produce electricity is a challenge because of high prices in fuel. Solar panels which are portable should be encouraged for use in homes to augment potential shortfalls and high electricity tariffs faced by consumers. To solve this challenge of electricity crisis, Ghana needs to exploit the most abundant, renewable and sustainable energy source in the tropics which solar energy is one. According to earlier work, it was estimated that in 90 minutes, the amount of energy from sunlight that strikes the earth is enough to provide the earth with all its energy needs for a year (US Department of Energy, 2016, para. 1). Solar energy is a substitute boundless energy source which can be utilized for electricity production. Research has also discovered that Azo dyes with broad absorption bands in UV-Vis region, reap a lot of photons which can aid device performance in electricity production.

1.8 Aim and Objectives

The main aim of the research is to synthesize, purify and characterize azo dyes as sensitizers for possible application in dye-sensitized solar cells (DSSCs)

The specific objectives are to:

i. Synthesize 4-(phenylazo)-1-naphthol (Dye 1), 1-(Phenyldiazenyl)-2-naphthalenol (Dye 2), 5-phenyldiazenyl-8-hydroxyquinoline (Dye 3) , 2-hydroxyl-5-bis(Phenyldiazenyl)benzoic

acid (Dye 4), 5-bis(Phenyldiazenyl)-8-hyrdoxyquinoline (Dye 5), 1-bis(Phenyldiazenyl)-2-naphthalenol (Dye 6), 1-tri(Phenyldiazenyl)sulphanilic acid-2-naphthalenol (Dye 7), 2-hydroxyl-5-tris(Phenyldiazenylsulphanilic acid) (Dye 8)

ii. Purify the synthesized dyes by recrystallization

iii. Characterize the dyes using electronic melting point apparatus, Ultraviolet–Visible (UV-Vis) spectroscopy, nuclear magnetic resonance spectroscopy (NMR), Fourier Transform Infrared (FTIR) spectroscopy and cyclic voltammetry

iv. Compare results of characterizations to that of the standard inorganic ruthenizer 535-bisTBA (N719) dye

CHAPTER TWO

LITERATURE REVIEW

2.0 Overview

The chapter contains a review of literature related to the study and the theoretical frame work related to the important aspect of the study. The literature review discussed theoretical issues of History of azo dyes, General synthesis and mechanism of the reaction of azo dyes, Band Theory, Spectral and chromophoric absorption in azo dyes, cyclic voltammetry and photovoltaic. The chapter ends with the empirical literature on dye sensitized solar cells of the study and a conceptual framework mechanism of the synthesis of azo dyes.

2.1 Theoretical framework

2.2 History of Azo dyes

W. H. Perkin discovered Mauveine A in 1856 according to Meth-Cohn and Travis (1995), this was the first synthetic organic dye. From that time, many synthetic dyes have been prepared. For example azobenzothiazolyl dyes (Pavlovic etal, 2009) and acridine dyes (Halabieh, Ozzy & Barrett, 2004). In 1987 Zollinger reported that over 735 tons of synthetic dyes are produced annually (Zollinger, 1987). Nowadays, dyes are widely used in biological, environmental and analytical sciences (Sameiro, Maia & Goncalves, 2001). Most dyes are classified into types according to their chemical structure or application method and functional groups present in a molecule.

The biggest single group of dyes which have been manufactured are the azo dyes, all of which contain the -N=N- functional group attached directly to aromatic rings or aliphatic groups (Bansal, Singh & Sud, 2010). More than 50 % of the commercial dyes belongs to the class of azo dyes. Azo dyes provide colourful appearance. However, synthesized azo dyes are supplied in

oranges, reds and yellows than other colours. These colours are more preferred in the leather and textiles industries. Azo dyes provide brighter and greater intensity colours far than the most common dye class (anthraquinones). The advantage that azo dyes have over other dyes is their low cost and easy synthesis route in their manufacture.

2.3 Azo dye Formation: Direct method

According to Mchale (2008), azo dyes are synthesized in two steps: diazotisation and coupling. Conventional acid/ base catalysed reactions are effective in the synthesis of azo dyes. Diazotisation is carried out by protonating the compound under acidic conditions at a low temperature and the diazo compound is then coupled with the nucleophile under basic conditions (Carey & Sundberg, 2001). The mechanism for diazotisation and coupling is shown in the Scheme below.

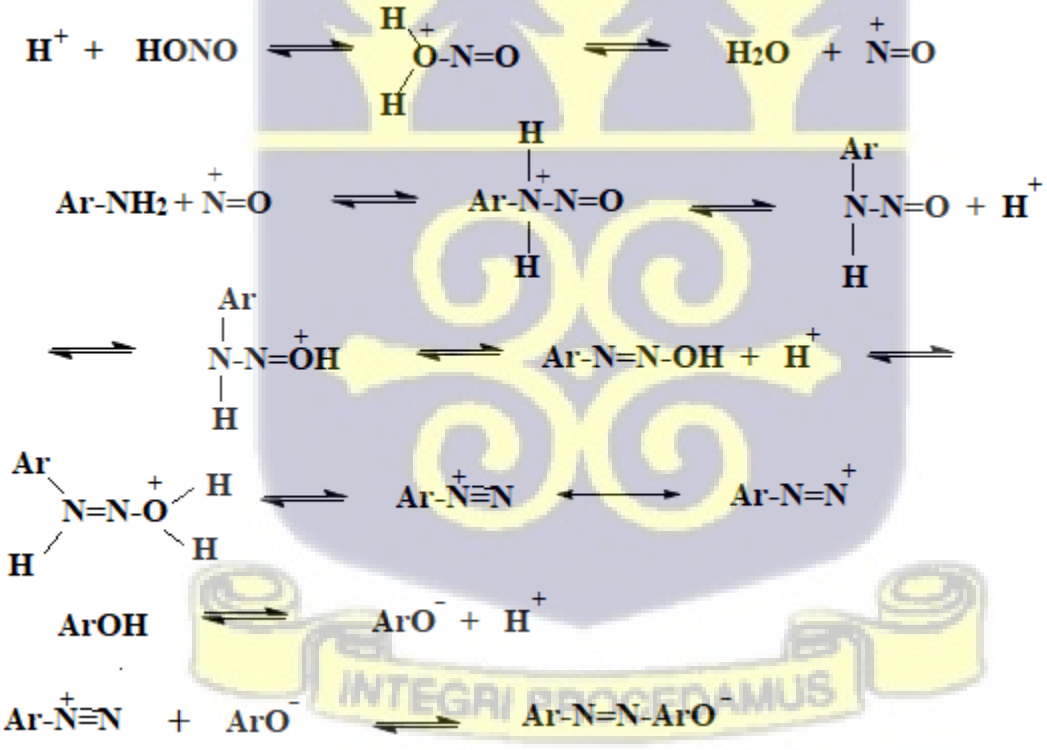

Scheme 2.1 General reaction mechanism for diazotization and coupling of azo dyes

The lengthy conjugation in azo dyes absorb light in the UV-Vis region of the electromagnetic radiation. The starting materials used for the synthesis of azo dyes are easily available and have low cost. This makes it possible for mass production. The reactions are usually performed at lower temperatures (0-5 ^{o}C) and the common solvent is water. It has low impact on the environment due to its ability to decompose easily.

2.4 General Synthesis and Mechanism of the reactions

The general synthesis pattern is demonstrated below:

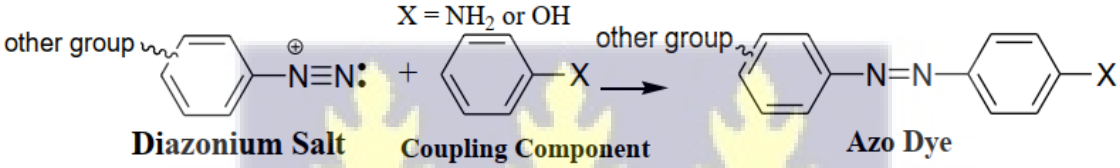

Scheme 2.2 Formation of azo dyes from diazonium salts and coupling agent

2.5 Band Theory

Band theory defines atoms in metals as having orbitals that are overlapping and form bands. Valence shell orbitals form the valence band whereas empty shells form the conduction band (see Figure 2.2). Electron excitation from the valence band to the conduction band occurs with the help of external stimuli (heat, light etc.).

The description of the structure of a band in a solid are called energy bands as described in solid state physics, where you can have an electron in the solid ("allowed bands") and ranges where the electrons maybe absent which is called band gaps ("forbidden bands"). Band theory explains the way electrons behave in solids thereby suggesting energy bands presence in solids. The theory is able to explain many physical properties of solids based

on material's band structure.

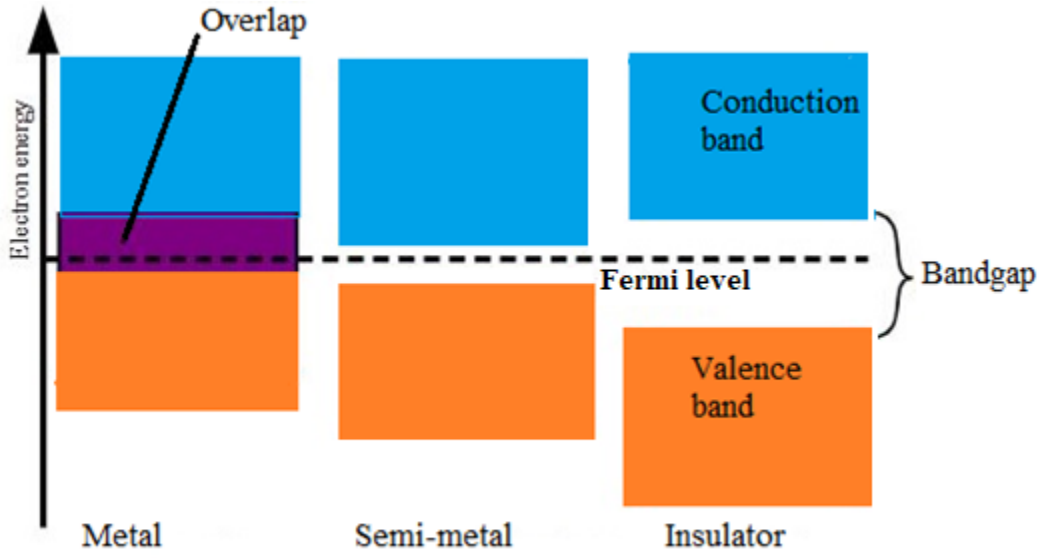

Figure 2.1 Solid materials and their band gap region

Conductors are solids having atomic valence orbitals overlapping with the conduction bands (see Figure 2.1). Insulators have a wider gap between the bands (conduction and valence bands). The intermediate state are semiconductors. The energy distance (gap) between the bands of conductors are diminished with an electronic fermi level (electronic sea level at absolute zero or the energy of the least tightly bound electrons within a solid) lying within the conduction band (Jakubowski, 2010). The Fermi level is seen in Figure 2.1 as the energy level being occupied at a temperature of 0 K by the electron orbital. Therefore a fraction of the electrons move in the conduction band in the absence of an external stimuli. However, with a large energy gap between conduction and valence band, electrons in insulators are unable to excite into the conduction band. The term semiconductor was first coined by Alessandro Volta in 1782. Some semiconductors allow electrons to easily move to the conduction band with the aid of external stimuli. He described them as materials whose electric properties are characterized by a narrow energy gap with a fermi level between the valence and conduction band.

2.6 Energy Gap of Synthetic Organic Molecules

The design of synthetic semiconducting organic molecules focuses on the narrowing of the HOMO-LUMO energy gap (Scharber et al, 2006). Further research has shown that the ideal energy gap for synthetic semiconducting organic molecules should lie within 1.0 and 2.0 eV (Yeats, Taylor & Skabara, 2018).This ideal range demonstrated a 30% to 77% absorption of incident photons in UV-visible light. The Figure 2.4 shows the relationship between the Energy gap of solid materials.

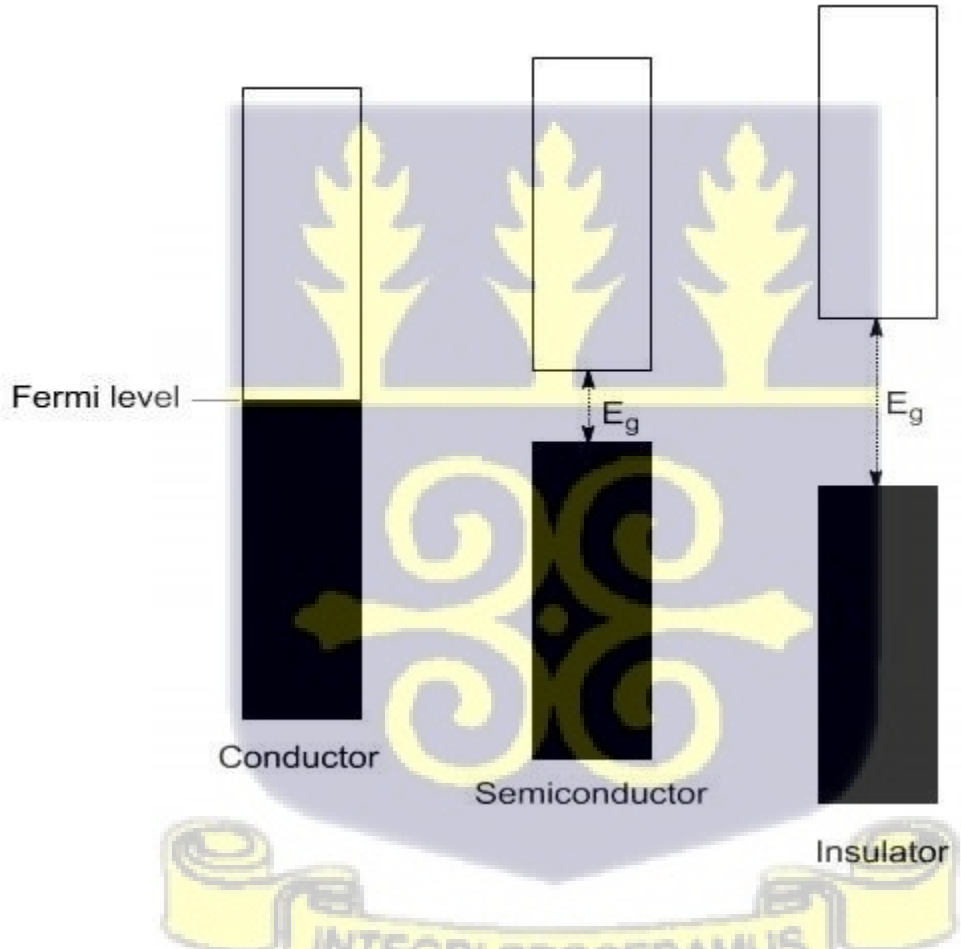

Figure 2.2 Electronic band structure of conductors, semiconductors and insulators.

2.7 Spectral Chromophoric Absorptions in Azo dyes

Absorption has been defined by Louis and Fieser as vibration of molecular electrons which can result in exciting light rays of specific wavelengths. Electrons will respond and absorb light energy of short wavelength and high frequency. As a results of this, there is excitation in which electrons become more mobile. The accumulation of conjugated centres of unsaturation in the molecule also causes excitation at the molecular level. Accordingly, n-π*, π-π* and n-σ* transitions will happen in molecules attacked by UV light (Aziz et al., 2019).Transitions for n-π* and π-π* have strong absorptions around 263 nm and 354 nm respectively. This can results in absorption of radiant energy in the UV-Vis region. Unsaturation and conjugation in dyes are essential for light absorption. Chromophoric regions in azo dyes responsible for absorption occurs normally in a wavelength from 250 nm to 1000 nm.

Table 2.1 Chromophores of Organic Compounds and their Absorption wavelengths in the UV-Vis regions

GROUP	EXAMPLE	WAVELENGTH(λ_{max}) , nm	INTENSITY(AU)
C=C	Ethylene	193	10,000
C≡C	Acetylene	173	6,000
C=N	Acetoxime	190	5000
C≡C	Acetonitrile	<160	---
C=O	Acetone	271	15.8
CHO	Acetaldehyde	293	11.8
COOH	Acetic acid	204	40

$CONH_2$	Acetamide	208	---
N=N	Diazomethane	410	1,200
N=O	Nitrosobutane	300, 665	100, 20
NO_2	Nitromethane	271	12
O=N-O	Octyl nitrite	230, 370	2,200, 55
ONO_2	Ethyl nitrite	270	12

Conjugations in unsaturated compounds having double bonds, triple bonds and carbonyl or nitro groups give rise to high intensity band in the region 200-230 nm, representing a bathochromic displacement of 15-45 nm with respect to the ethylene bond. Two distinct bands are often observed; for, α , β- unsaturation ketones which have a maximum of high intensity at 230-270 nm and another of low intensity within 300-330 nm. This is characteristic for conjugated unsaturation of the benzene rings to produce colour to the azodyes. Table 2.2 shows absorption of some conjugated systems.

Table 2.2 Absorption characteristics of some simple conjugated systems

SYSTEM	EXAMPLE	WAVELENGTH(λ_{max}) , nm	INTENSITY
C=C-C=C	Butadiene	217	20,900
C=C-CH=O	Crotonaldehye	217, 321	16,000; 19.5
$C=C-CO_2H$	Crotonic acid	200;250	10,000;100

Aromatic ring	Benzenze	255	230
$C_6H_5CH=CH$	Styrene	244	12,000
C=C-C=C-C=C	Octatrienol	26.5	53,000
C=C-C=C=CH=O	Sorbaldehyde	26.3	27000

Semiconducting organic molecules have the ability to absorb photons in the UV-visible region (200-800 nm). The delocalised π-electron system in the molecule undergo transitions because of the absorptions in the UV-visible region. These electrons generally experience π-π* transitions and occasional *n*-π* promotion in the UV-visible region. The HOMO-LUMO energy gaps are estimated by finding the leading edge of the absorption spectrum. Figure 2.4 below shows the possible electronic transition of organic molecules used for sensitizers in DSSCs.

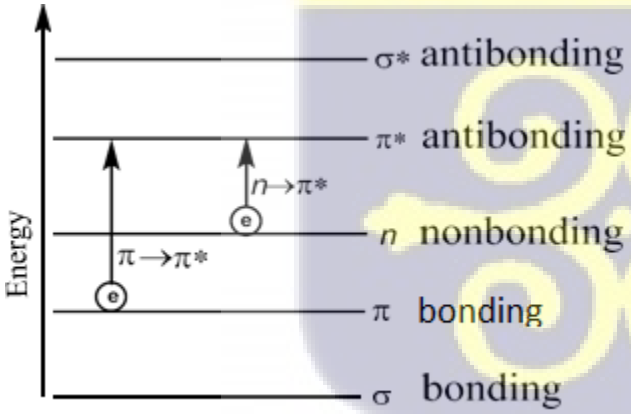

Figure 2.3 Possible electronic transition of semiconducting organic molecules.

2.8 Cyclic Voltammetry

Cyclic voltammetry is a highly utilized electrochemical procedure to measure the reduction and oxidation of an electroactive species (Bard & Faulkner, 2000). Measurements gotten from Cyclic voltammetry are used to study the diffusion and kinetic effects of some substances using plain or Nano-modified electrodes (Nicholson, 1965; Keeley & Lyons, 2009). These systems comprise of a three electrode cell submerged in a stationary solution. Working electrode, reference electrodes and counter electrode are positioned within close proximity to each other in a closed cell. Cyclic voltammetry is a simple, powerful and rapid technique that is used to characterize electrochemical behaviour of analytes that been oxidized or reduced electrochemically. The reduction and oxidation results in HOMO and LUMO energy transition respectively. The study of electron transfer in cyclic voltammetry is as a results of concurrently activating molecules in which electrons are promoted and transferred subsequently through a photocatalytic chemical reactions. The data derived from cyclic voltammetric analysis of compounds details how the electron transfer in an oxidation and reduction reaction process.

2.9 Photovoltaic

Photovoltaic converts solar energy into electricity using semiconductor materials. There are three different categories of photovoltaics. The energy conversion efficiency for both the first and second generation of solar cells is limited by the Schockley-Queisser limit of 31 % power efficiency for single band gap solar cells (Shockley & Queisser, 1961). The limited power efficiency results from energy losses incurred by relaxation of photons with energies higher than the band gap of the semiconductor, and the fact that photons with energies lower than the band gap will not contribute to the power efficiency.

The first generation of solar cells is semiconductor p-n junction solar cells, such as silicon. Silicon solar cells dominate the photovoltaic market today, and certified efficiencies of about 25 % have been obtained for single crystal silicon cells (US Department of Energy). The cost is, however, relatively high for these solar cells, because of the high energy required for the purification process of the material.

The second generation of solar cells focuses on reducing the cost of the first generation by using thin-film technologies. Thin film solar cells are based on thin layers of various semiconductor materials, such as amorphous silicon, cadmium telluride (CdTe), or copper indium gallium diselenide (CIGS). CIGS solar cells have certified efficiencies of about 20 %(US Department of Energy). The thin film solar cells require less material, but the use of rare elements may limit large-scale production of the devices. The energy payback time, i.e. the time the system has to operate to recover the energy that went into making the system, is as high as four years for silicon, and three years for thin film solar cells, respectively (US Department of Energy).

The third generation of solar cells is based on devices that can exceed the Schockley-Queisser limit. This generation of solar cells include multi-junction (tandem) solar cells and other new evolving technologies that use principle of hot and multiple electron carriers. Dye-sensitized solar cells, which are the main focus of this thesis, is a technology between the second and third generation of solar cells.

2.10 Dye sensitized Solar Cells

In 1991, Professor Michael Gratzel demonstrated dye-sensitized solar cells (DSSCs) for the first time (Gratzel, Nazeeruddin & Baranoff, 2011). DSSCs have been a point of attention to both

researchers and industries worldwide. The light absorption from the sun's energy brings excitations in molecule of materials than in the free electrons and holes is the basic variation between solar cells with organic sensitizer and regular inorganic photovoltaic (IPV) cells. Organic solar cells (OSCs) are preferred in current years because its merit as compared to inorganic solar cells. Organic solar cells have environmentally friendly, low cost, light and flexible. Also, in solar energy production, excitation in an OSC semiconductor is described as a tightly coulombicly bound electron hole pair. Because of the strong binding energy and electrical neutrality between the hole and the electron it is described as a mobile excited state (Halls and Friend, 2001). Research by Grätzel and Moser (2005) showed that organic compounds like azodyes combines the functions of light absorption and charge (hole) transport in a single material to produce electrical energy. Nazeeruddin. Pechy and Gratzel(1997) also used Ru based metal complex dyes (e.g. N3, N719, Z907) and showed that there is efficiencies of more than 10%; these possess many desirable optical and electronic properties like a broad absorption spectra, suitable excited and ground state energy levels which have good chemical stability but have low molar extinction coefficient. Other metal ion complexes like Re, Pt, Os and Cu complexes have been developed and used as sensitizers in DSSCs (Islam et al, 2001). Further studies has showed that modular architecture of the DSSC thus enables functions such as electron transport, light absorption and hole transport to be handled separately. Given that, by introducing systematic variations of the substituent groups in the dye, this can improve the light harvesting and electron injection capabilities among other properties, various classes of dyes (metal-free and inorganic-based) have been investigated ranging from coumarins, carbazoles, indolines and triphenylamines(Mahmood, 2016). Organic sensitizers without metallic elements have been used to replace the expensive ruthenium based sensitizers and to improve the electronic properties of devices. The efficacy of these sensitizers is still low when

compared to devices based on ruthenium-based dyes, the efficacy and performance can be improved by the proper selection or tuning of the designing components (Andualem & Demiss, 2018). A study conducted by Kaung etal in the university of Yangon showed that a film of solar cell with common garden Hibiscus dye showed a solar energy conversion efficiency (η) under sunlight reached 1% with I_{SC} value of 1.38mAcm^{-2} , V_{OC} value of 0.46V, and a fill factor (ff) value of 0.67(Kaung etal, 2014). The continuous effect in looking for affordable organic solar energies, among which DSSCS have far demonstrated the highest energy conversion efficiency as best candidates for use in the future.

2.11 Current Approaches and Trends in Dye sensitized solar cells

Nevertheless, another way to optimize the performance of the DSSCs has been started by adding the energy relay dyes (ERDs) to the electrolyte (Margulis et al, 2013); inserting luminescent chromophores or phosphorescence, such as the use of rare-earth doped oxides (Jiang et al. 2014) into the DSSC; and coating a luminescent layer on the glass of the photoanode (Wang, 2015) In the addition of ERDs to the electrolyte or to the HTM, some highly luminescent fluorophores have to be chosen. The major role of ERD molecules in DSSCs is to absorb the light that is not in the primary absorption spectrum range of the sensitizing dye and then transfer the energy non-radiatively to the sensitizing dyes by the fluorescence (Forster) resonance energy transfer (FRET) effect. There has been an improvement in the external quantum efficiency of 5 to 10% in the spectrum range from 400 to 500 nm has been demonstrated by Siegers and colleagues. Recently, Lin et al (2017), reported the doping of 1,8-naphthalimide (N-Bu) derivative fluorophore directly into a TiO_2 mesoporous film with N719 for application in DSSCs in which the N-Bu functioned as the FRET donor and transferred the energy via spectral down-conversion to the N719 molecules (FRET acceptor). An improvement of the PCE from 7.63 to 8.13% under 1 sun (AM 1.5)

illumination was attained by the cell. Similarly, Prathiwi et al (2017). moulded a DSSC by adding a synthetic dye into the natural dye containing anthocyanin (from red cabbage) in 2017. They prepared two different dyes at different volumes, i.e., anthocyanin dye at a volume of 10 ml and combination dyes at a volume of 8 ml (anthocyanin): 2 ml (N719 synthetic dye), respectively. There was an observation in conversion efficiency up to 125 %, because a single anthocyanin dye achieved a conversion efficiency of 0.024 % whereas for the combination dye 0.054 % conversion efficiency was achieved. Thus, greater photon absorption took place and the electrons in excited state were also increased to enhance the photocurrent. Recent trend shows that cocktail dyes are also developing as a new trend in DSSCs. Chang et al (2013) achieved a $\eta = 1.47\%$ when chlorophyll dye (from wormwood) and anthocyanin dye (from purple cabbage) as natural dyes were mixed together at volume ratio of 1:1 (Chang, 2013) while the individual dyes showed lower conversion efficiencies. Puspitasari et al (2017) fabricated different DSSCs by mixing the three different natural dyes as turmeric, mangosteen, and chlorophyll. The highest efficiency of 0.0566% was attained for the mixture of the three dyes, where the absorbance peak of the mixed dyes was observed at 300 nm and 432 nm. Likewise, Lim and co-workers have achieved a 0.085% of efficiency when xanthophyll and chlorophyll dyes were mixed together (Lim, 2015). In 2018, Konno et al(2018). studied the PV characteristics of DSSCs by mixing different dyes and observed highest $\eta = 3.03\%$ for the combination dye "D358 + D131," respectively (Zhang, 2018)

An approach used to enhance the performance of DSSCs is plasmonic effect. Surface plasmon resonance (SPR) is resonant oscillation of conduction electrons at the interface between negative and positive permittivity material stimulated by incident light. In 2013, Gangishetty and co-workers synthesized core-shell NPs comprising a triangular nanoprism core and a silica shell of variable thickness. SPR band centered at ~ 730 nm was observed for the nanoprism Ag particles,

which overlapped with the edge of the N719 absorption spectrum very well. They found the incorporation of the nanoprism Ag particles into the photoanode of the DSSCs yielded a 32% increase in the overall PCE (Gangishetty, 2013). Hossain et al. used the phenomenon of plasmonic with different amounts of silver nanoparticles (Ag NPs) coated with a SiO_2 layer prepared as core shell $AgSiO_2$ nanoparticles ($AgSiO_2$ NPs) and studied the effect of SiO_2-encapsulated Ag nanoparticles in DSSCs. They found the highest PCE of 6.16% for the photoanode incorporated 3 wt% $AgSiO_2$; the optimal PCE was 43.25% higher than that of a 0 wt% $AgSiO_2$ NP photoanode (Hossain,2016) However, a simultaneous decrease in the efficiency with further increases in the wt% ratio, i.e., for 4 wt% $AgSiO_2$ and 5 wt% $AgSiO_2$, was observed. This decrease for the excess amounts of $AgSiO_2$ NPs was attributed to three reasons: (i) reduction in the effective surface area of the films, (ii) absorption of less amount of the dye, and (iii) an increase in the charge-carrier recombination (Ihara, 2010) After analyzing the nyquist plots, they have found a decreased diameter of Z_2 monotonically as the $AgSiO_2$ NP content increased to 3 wt% and R2 decreased from 10.4 to 6.64 Ω for the conventional DSSC to the 3 wt% $AgSiO_2$ NPs containing DSSC. Jun et al (2016). said that quantum-sized gold NPs to can be used to create plasmonic effects in DSSCs

2.12 Conceptual Framework

2.13 Reaction Mechanism

The reaction mechanism of forming azo dyes has been described below:

Step 1: hydrochloric acid is reacted with sodium nitrite to produce nitrous acid. This is further protonated under acidic medium for water to be removed and yield nitrosonium ion.

Step 2: An electrophilic nitrosonium ion produced in step 1 reacts with an aromatic amine forming a nitrosoamine.

Step 3: A tautomeric reaction occurs that results in a proton transfer nitrosoamine.

Step 4: OH group reacts with the hydrogen ion under acidic medium to remove water for the diazonium salt to be formed.

Step 5: An electrophile attacks the diazonium salt. The electrophile is an electron-rich coupler such as an aniline, sulphanilic acid or phenol through an electrophilic aromatic substitution reaction. The para directors, $-NH_2$ or -OH group direct the aryl diazonium ion to the para site if unoccupied. In case the para position is occupied then it moves to the ortho sites.

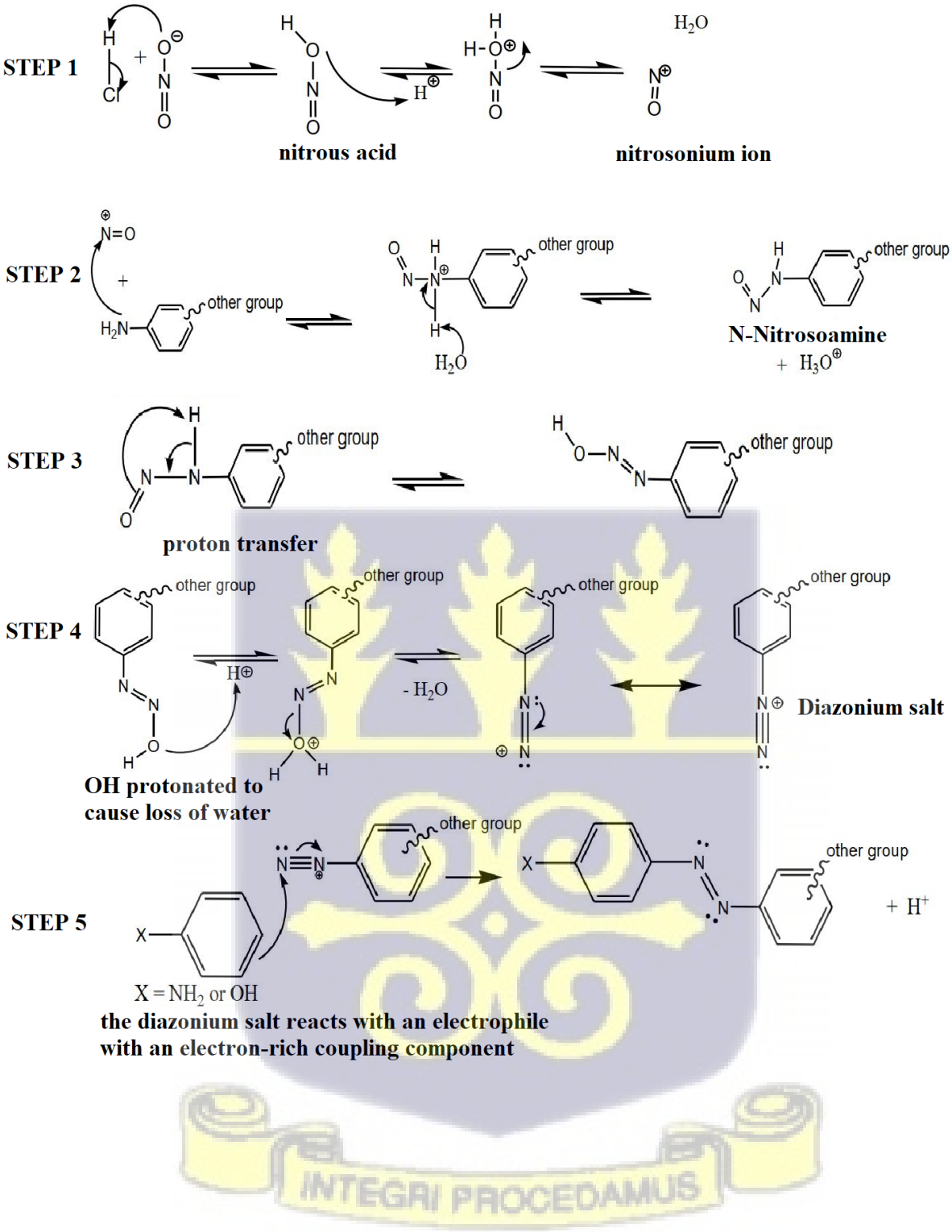

CHAPTER THREE

3.0 METHODOLOGY

This chapter explains the methodology used in the study. The synthesis and characterization of azo dyes and measurement of their optical properties are explained in this chapter. The various characterization techniques used, operation principles, equipment and sample preparation are described in this chapter.

3.1 Chemicals and Reagents

Ethanol (96%, Inner Mongolia Pulis chemicals), methanol (99.85%), ethyl acetate(99.5%), acetone(99.5%), salicylic acid (99.5%), dichloromethane (DCM) (99.8%), aniline (99.9%), hydrochloric acid (98%), tetraoxosulphate (VI) acid (98%), 2-naphthol (99%), 1-naphthol (99%), sodium nitrite ($NaNO_2$) (97%), sodium acetate (99%), sodium chloride(99%), (all from Fisher Scientific Company, USA). All solvents used were of the analytical grade.

3.2 Apparatus and Materials

UV-Vis Spectrophotometer (Shimadzu Scientific Instruments Inc, Maryland, USA), and Electro thermal melting point apparatus (LabX in Midland, ON, Canada), FT-IR Spectrometer and NMR (Bruker, Massachusetts, United States) were used for analysis. 12 Beakers (250ml), 6 Boiling tubes, Filter paper(Whatman, medium size), Buchner funnel , Aluminum foil, Stirring rod-1, 2 Conical flasks (250 ml) and 5 Volumetric flasks (250 ml) were used for synthesizing the dyes. An ice bath was used to provide a temperature range of 0-5^{0}C.

3.3.0 Synthesis and Purification of Azo Dyes

3.3.1 4-(phenylazo)-1-naphthol - Dye 1

Aniline (4.57 g, 49 mmol) was dissolved in 15 mL of 50% H_2SO_4 which was cooled to reach a temperature range within 0–5 ^oC. A solution of $NaNO_2$ (4.0 g, 58 mmol in 15 mL of water) which has been cooled was added dropwise within a temperature range of 0-5 ^oC to the resulting mixture. A diazonium salt was produced after stirring the mixture for about 30minutes. A previously prepared solution of 1-naphthol (7.2 g, 50 mmol of 1-naphthol in 60 mL of 20 % NaOH) was cooled below 5 ^oC in alkaline medium and added slowly in drops to the diazonium salt solution. An azo dye was formed which was sticky in nature. Cold water was added dropwise to reduce the sticky mass formation of azo dyes.

The reaction mixture was thoroughly mixed by stirring for about 3hours and kept at Room Temperature for an hour. Sodium acetate was used to adjust the pH to 7-7.5 range. The dye that was precipitated out of the mixture was filtered. The filtrate was further washed with cold water. It was further recrystallized from an acetone and alcohol ratio mixture of 1:1 and dried in ordinary air resulting in a solid compound.

3.3.2 1-(Phenyldiazenyl)-2-naphthalenol – Dye 2

Same method for synthesizing Dye 1 was used and the coupling agent was 2-naphthol (7.2 g, 50 mmol of 2-naphthol in 60 mL of 20 % NaOH).

The same purification procedure for Dye 1 was used.

3.3.3 5-phenyldiazenyl-8-hydroxyquinoline – Dye 3

Same method for synthesizing Dye 1 was used and the coupling agent was 8-hydroxyquinoline (2.00 g, 25 mmol in 10 mL ethanol and in 10 %).

The same purification procedure for Dye 1 was used.

3.3.4 2-hydroxyl-5-bis(Phenyldiazenyl)benzoic acid – Dye 4

Same method for synthesizing Dye 1 was used and the coupling agent was 2-hydroxy-5-phenyldiazenylbenzoic acid (2.00 g, 25 mmol in 10 mL ethanol and in 10 %).

The same purification procedure for Dye 1 was used.

3.3.5 5-bis(Phenyldiazenyl)-8-hyrdoxyquinoline – Dye 5

Same method for synthesizing Dye 1 was used and the coupling agent was 5-phenyldiazenyl-8-hyrdoxyquinoline (0.50 g, 25 mmol in 10 mL ethanol and in 50 ml of 10 % NaOH).

The same purification procedure for Dye 1 was used.

3.3.6 1-bis(Phenyldiazenyl)-2-naphthalenol – Dye 6

Same method for synthesizing Dye 1 was used and the coupling agent was 1-(Phenyldiazenyl)-2-naphthalenol (2.00 g, 25 mmol in 10 mL ethanol and in 50 ml of 10 % NaOH).

The same purification procedure for Dye 1 was used.

3.3.7 1-tri(Phenyldiazenyl)sulphanilic acid-2-naphthalenol - DYE 7

Sulphanilic acid (0.8 g, 49 mmol) was dissolved in 15mL of 50 % H_2SO_4 which is further cooled to reach a temperature range within 0-5 ^oC. A solution of $NaNO_2$ (4.0 g, 58 mmol in 15 mL of water) which has been cooled was added in drops at within a temperature of 0-5 ^oC to the resulting mixture. A diazonium salt was produced by stirring the mixture for about 30minutes. A previously prepared solution of 1-bis(Phenyldiazenyl)-2-naphthalenol (1.00 g, 25 mmol in 10 mL ethanol and in 50 ml of 10 % NaOH) which was cooled below 5 ^oC in alkaline medium was added slowly in drops to the diazonium salt solution. An azo dye was formed which was sticky in nature. Cold water was added in drop wise to reduce the sticky mass formation of azo dye.

The same purification procedure for Dye 1 was used.

3.3.8 2-hydroxyl-5-tris (Phenyldiazenylsulphanilic acid)benzoic acid - Dye 8

Same method for synthesizing Dye 7 was used and the coupling agent was 2-hydroxyl-5-bis(Phenyldiazenyl)benzoic acid (1.00 g, 25 mmol in 10 mL ethanol and in 50 ml of 10 % NaOH).

The same purification procedure for Dye 1 was used.

3.4 Structural, Physicochemical and Electrochemical Analysis of Synthesized Dyes.

The synthesized dyes were characterized using the following physical and chemical analysis techniques: Stuart electrothermal melting point apparatus, UV-Vis spectrophotometer, FT-IR spectrophotometer and Cyclic Voltammetry.

3.5 Melting point determination of synthesized dyes

A glass capillary melting point tube with one end sealed and the other end open was used. The end that was opened was jabbed with a well dried sample of the DYE 1 to be measured. This was inverted and gently tapped for the solid sample to fall to the end that is sealed. This was done to make sure that no spaces were left in the capillary tube. The process was repeated to load the dye sample to a height 2-3mm of the glass capillary tube. The tube jabbed with the sample was inserted into a slot behind the viewfinder of a melting point apparatus. The Electrothermal melting point apparatus was turned on and an appropriate heating rate of 1°C was set. The temperature range of the device has maximum temperature limit of 300 °C. When a melt a starts, the apparatus starts to heat at the pre-programmed rate until the melting was complete or until the device reaches a pre-determined end temperature. After determining the melting point of the sample, the instrument is allowed to cool until it reaches 50°C. DYE 1 was heated at a medium rate to determine an approximate melting point. The process was repeated with another sample after allowing the

apparatus to cool and used the settings to perform a more precise melting point. The fresh sample was loaded into the glass capillary tube and a second melting point was taken. The third melting point was taken for the same Dye 1. This method was repeated for all the remaining samples (DYE 2, DYE 3, DYE 4, DYE 5, DYE 6, DYE 7 and DYE 8).

Figure 3.1. Measurement of sample using Stuart Electrothermal melting point apparatus

3.6 Fourier Transform-IR Spectroscopy determination

Acetone was used to clean the Attenuated Total Reflection (ATR) crystal before measurement. The dried Dye sample of about 0.5 g was placed on the ATR crystal by a clean spatula. Pressure was applied by the pressure handle. Several scans were performed on the computer within a frequency range of 4000 cm^{-1} – 400 cm^{-1}. A resultant spectrum for Dye 1 was obtained and saved on the computer for further processing and functional group elucidation. This process was repeated for all the dyes including the reference dye N719.

3.7 UV-Vis Spectrophotometry

0.1 mM solutions of the dyes 1 to 8 and the reference dye were prepared using ethanol as solvent. The UV-Vis device was connected to a computer and turned on for the programme to boot. Two glass cuvettes were well cleaned and air dried. About 5 ml of the blank (ethanol) was poured into each of

the cuvettes with a clean dropper. The clear sides of the cuvettes were cleaned with a white tissue to remove fingerprints and residue of the blank. This was placed in the measurement chamber and scanned to set baseline correction. The blank in the second cuvette at the lower side of the UV-Vis spectrophotometer was removed and discarded. About 5 ml of DYE 1 solution was poured into the cuvette. The clear sides of the cuvettes were cleaned with a white tissue to remove fingerprints and residue of sample. The filled cuvette was placed in the UV-Vis device. The start scan was selected for a wavelength from 250 nm to 800 nm. A UV-Vis spectrum was produced and saved on the computer. The process was repeated for the absorption spectrum of each dye purified (DYE 2, 3, 4, 5, 6, 7 and 8) were measured using a UV-1800 double beam spectrophotometer. For comparison, the absorption of the standard inorganic ruthenizer 535-bisTBA (N719) dye was also measured. Each dye's absorption spectrum was measured. The maximum absorption peaks (λ_{max}) from the absorption spectrum of each dye was used as the excitation wave length for their fluorescent measurement.

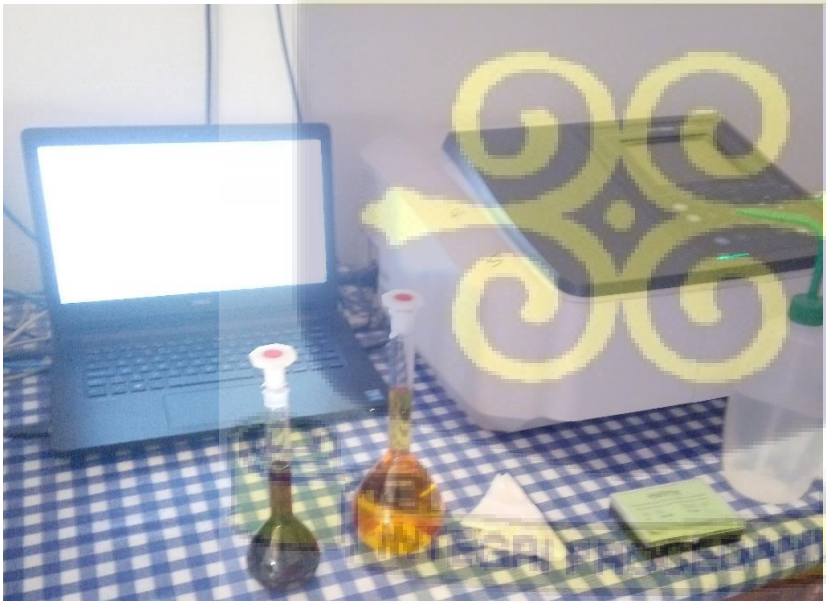

Figure 3.2. Setup of UV-Vis Spectrophotometry Workstation ready for UV-Vis measurement.

3.8 Cyclic Voltammetry (CV) Measurement

The electrochemical properties of the eight dyes were investigated by using a potentiostat galvanostat and compared with the standard **N719** dye. Acetonitrile (CH_3CN) was used as the preparation solvent. A 10^{-4} M solution of the **DYES** and **N719** dye were prepared. CV was measured using a three-electrode system consisting of a glassy carbon working electrode, platinum counter electrode and Ag/AgCl reference electrode at a scan rate of 0.1 V/s. The image (Figure 3.3) is a computer controlled Instrument CS150 Metrohm Autolab B. V. NOVA 1.11 Electrochemical Workstation. A solution of 0.1 M of tetrabutylammonium hexafluorophosphate ($TBAPF_6$) was used as a supporting electrolyte, in acetonitrile solution. All measurement were done in the Faraday cage to ensure background correction. Ferrocene was used as a reference standard for the measurements. All of the experiments were done at room temperature. The data obtained were referenced to the $E_{1/2}$ of ferrocene/ferrocenium (Fc/Fc^+) redox couple taking the HOMO of ferrocene to be -4.80 eV.

Figure 3.3. Setup of Electrochemical Workstation (Cyclic Voltammetry Instrument CS150 Metrohm Autolab B. V. NOVA 1.11) for CV measurement.

3.9 NMR Measurement

Residual ^{1}H in deuterated solvents was used to calibrate the NMR before experiments were performed. An amount of 5 mg of Dye 1 was dissolved in 2-3 ml of Deuterated chloroform ($CDCl_3$) containing Tetramethylsilane (TMS) as a reference material. NMR glass tubes of diameter 5mm were rinsed with acetone and dried with a blast of dry air. The prepared sample was filled into the NMR tube to the same height as the lock solvent and covered with a cap. The sample was labelled as DYE 1 on the cap. The sample was then placed in a sample holder and put into the NMR magnetic hole. This was allowed to drop into the magnetic chamber. The tube spins at 20 Hz (1200 rpm) while it was in the magnet. Eight scans were selected and performed on the Bruker programme. A generated spectrum was stored for processing. This process was repeated for all the remaining seven dyes. For ^{13}CNMR spectra, 100 mg of the Dye 1 was dissolved in 2-3 mls of Deuterated chloroform ($CDCl_3$). NMR glass tubes of diameter 5mm were rinsed with acetone then dried with a blast of dry air .Similar procedures for ^{1}HNMR were followed as above. After the number of scans a spectrum was generated and stored for processing in about 20-60 minutes. This process was repeated for all the remaining seven dyes to generate ^{13}CNMR spectra. The arrangement of the hydrogen and carbon atoms in the dyes were elucidated by ^{1}HNMR and ^{13}C-NMR.

CHAPTER FOUR

4.0 Results and Discussion

4.1 Synthesis, Purification and Characterization of Azo dyes

After synthesis and purification of the compounds, codes were given to the dyes and their physical properties (melting point, colour and nature) determined. Table 4.1 below describes the physical properties of the compounds.

Table 4. 1: Codes and physical properties of synthesized dyes.

Name Of Dye	**Code Name**	**Colour**	**Nature**	**Melting Point(**°C)	**Percentage Yield(**°C)
4-(phenylazo)-1-naphthol	DYE 1	Yellow	Powdery	180- 182	60.2%
1-(Phenyldiazenyl)-2-naphthalenol	DYE 2	Reddish-Brown	Powdery	202-205	76.7%
5-phenyldiazenyl-8-hydroxyquinoline	DYE 3	Dark brown	Powdery	103 - 105	68.7%
2-hydroxyl-5-bis(Phenyldiazenyl)benzoic acid	DYE 4	Dark brown	Powdery	112-114	77.2%
5-bis(Phenyldiazenyl)-8-hyrdoxyquinoline	DYE 5	Dark brown	Powdery	105-107	61.7%
1-bis(Phenyldiazenyl)-2-naphthalenol	DYE 6	Dark brown	Powdery	104 - 106	71.5%

1-tri(Phenyldiazenyl)sulphanilic acid-2-naphthalenol	DYE 7	Deep Brown	Powdery	118 -119	81.2%
2-hydroxyl-5-tris(Phenyldiazenylsulphanilic acid)benzoic acid	DYE 8	Brownish black	Crystal	106 - 109	68.7%
Di-tetrabutylammonium cis-bis(isothiocyanato)bis(2,2′-bipyridyl-4,4′-dicarboxylato)ruthenium(II)	N719 dye	Brownish-red	Crystalline powder	250 - 260	----------

The nature of DYE 1, DYE 2, DYE 3, DYE 4, DYE 5, DYE 6 and DYE 7 were powdery. DYE 8 had a crystal appearance. The melting point measured for DYE 1, DYE 2, DYE 3, DYE 4, DYE 5, DYE 6, DYE 7 and DYE 8 were 180-182 °C, 202-205 °C, 103-105 °C, 112-114 °C, 105-107 °C, 105-107°C, 104-106 °C, 118-119 °C and 106-109°C respectively. These observed temperature values are indicative of the stable nature of the prepared dyes due to higher temperatures. The observed melting point measured for the N719 dye was 250-260 °C. The melting point of this industrial standard dye was higher than all the eight synthesized dyes. This could be attributed to the higher molecular mass, increased bond strength and the presence of Ruthenium (II) ion presence in the N719 dye. The calculated percentage yield for DYE 1, DYE 2, DYE 3, DYE 4, DYE 5, DYE 6, DYE 7 and DYE 8 were 60.2 %, 76.7 %, 68.7 %, 77.2 %, 61.7 %, 71.5 %, 81.2 % and 68.7 % respectively.

4.2.0 FT-IR Spectroscopy Measurement

4.2.1 4-(phenylazo)-1-naphthol - Dye 1

Figure 4.1 depicts the IR spectrum of **DYE 1** and displays characteristic frequency regions of the dye. There was an O-H stretch vibration ranged from 3600 cm^{-1} to 3000 cm^{-1}**.** The spectrum below shows an O-H stretch vibration of R-OH with a high peak at 3401 cm^{-1} and a C=C stretch of alkenes at 1602 cm^{-1}. Also, a C-N= bend vibration of amines occurs at 1402 cm^{-1} and C-O stretch for an ester group occurs at 1273 cm^{-1}. The peaks around 756cm^{-1} and 681 cm^{-1} indicate aromatic regions in the compound which are meta disubstituted aromatic compound.

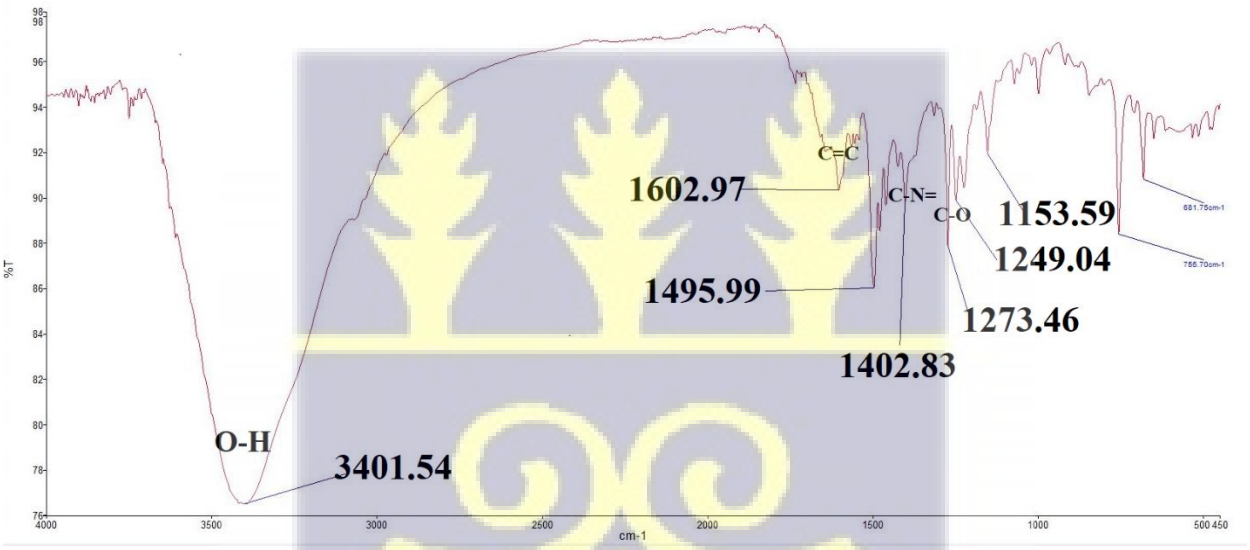

Figure 4.1 IR Spectrum of DYE 1

4.2.2 1-(Phenyldiazenyl)-2-naphthalenol – Dye 2

Figure 4.2 depicts the IR spectrum of **DYE 2** and displays characteristic frequency regions of the dye. There was a weak O-H stretch vibration ranged from 3250 cm^{-1} to 3100 cm^{-1}.The spectrum below shows O-H stretch vibration of R-OH with a small peak at 3200 cm^{-1} and a =C-H stretch for an alkene at 3028 cm^{-1}.The low intensity of the O-H stretch vibration might be due to the hydrogen bonding occurring between the hydrogen and the nitrogen in the azo bond. A =C-H bending for an aromatic ring was detected at 1446 cm^{-1} and C-N= stretch vibration at 1230 cm^{-1}.

The C-O group for a tertiary alcohol was detected at 1203 cm^{-1} and at at 748cm^{-1} was characteristic for an ortho disubstitution in aromatic compound.

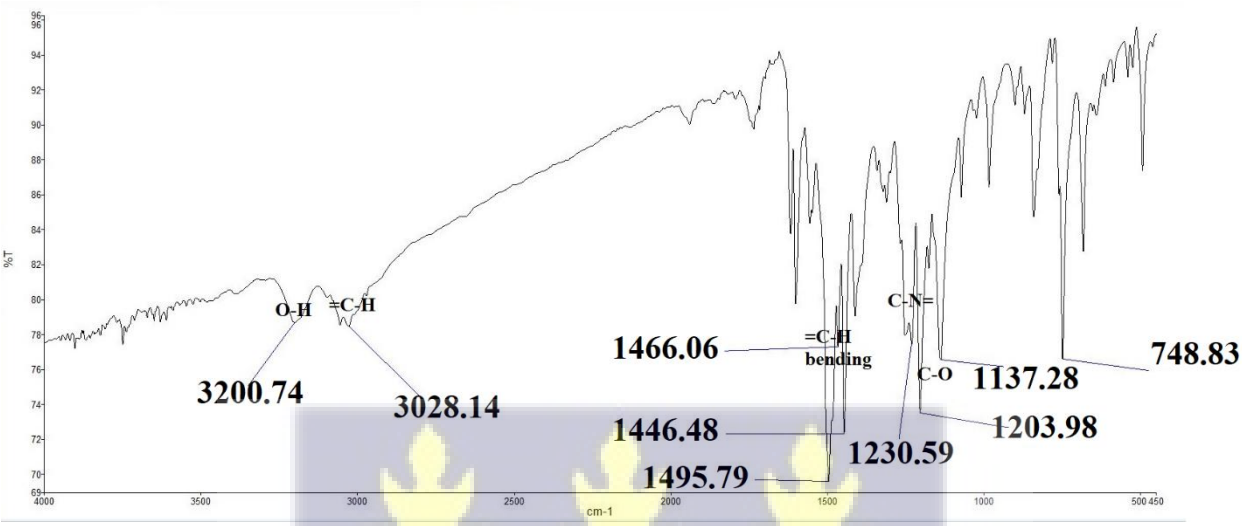

Figure 4.2 IR Spectrum of DYE 2

4.2.3 5-phenyldiazenyl-8-hydroxyquinoline – Dye 3

Figure 4.3 depicts the IR spectrum of **DYE 3** and displays characteristic frequency regions of the dye. There was an O-H broad vibration ranged from 3600 cm^{-1} to 3000 cm^{-1}. The spectrum below shows a high peak O-H stretch at 3369 cm^{-1} and C=N stretch group at 1541 cm^{-1}. Again, a N=N stretch for azo bond was detected at 1501 cm^{-1} and C-O stretch was detected at 1376 cm^{-1}. A C-N= stretch vibration also shows at 1285 cm^{-1}. Also, the spectrum shows a para and meta disubstitution in aromatic compound at 761cm^{-1}.

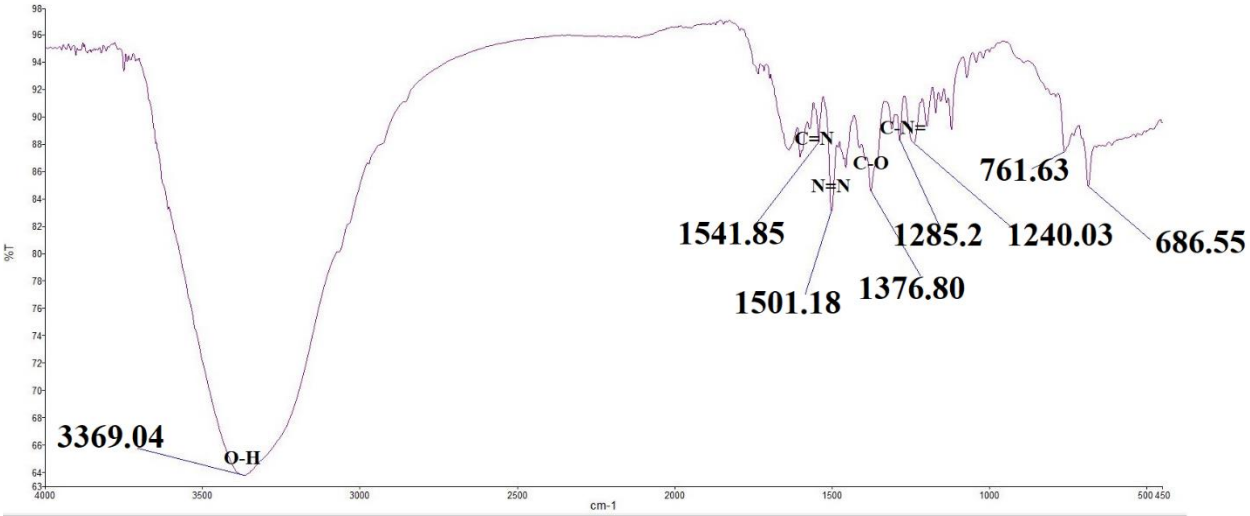

Figure 4.3 IR Spectrum of DYE 3

4.2.4 2-hydroxyl-5-bis(Phenyldiazenyl)benzoic acid – Dye 4

Figure 4.4 depicts the IR spectrum of **DYE 4** and displays characteristic frequency regions of the dye. There was an O-H broad stretch ranged from 3600 cm^{-1} to 3100 cm^{-1} The spectrum below shows O-H stretch vibration at a peak of 3392 cm^{-1} and a C=O stretch vibration of carboxylic acid at 1601 cm^{-1}. The spectrum also shows an indication for N=N stretch for azo bond at 1465 cm^{-1} and at 1443 cm^{-1} for C=C stretch for aromatic compound . It also shows C-N= stretch vibration at 1239 cm^{-1} and C-O stretch at 1195 cm^{-1}. An aromatic regions for a meta disubstitution is characteristic at 685cm^{-1}.

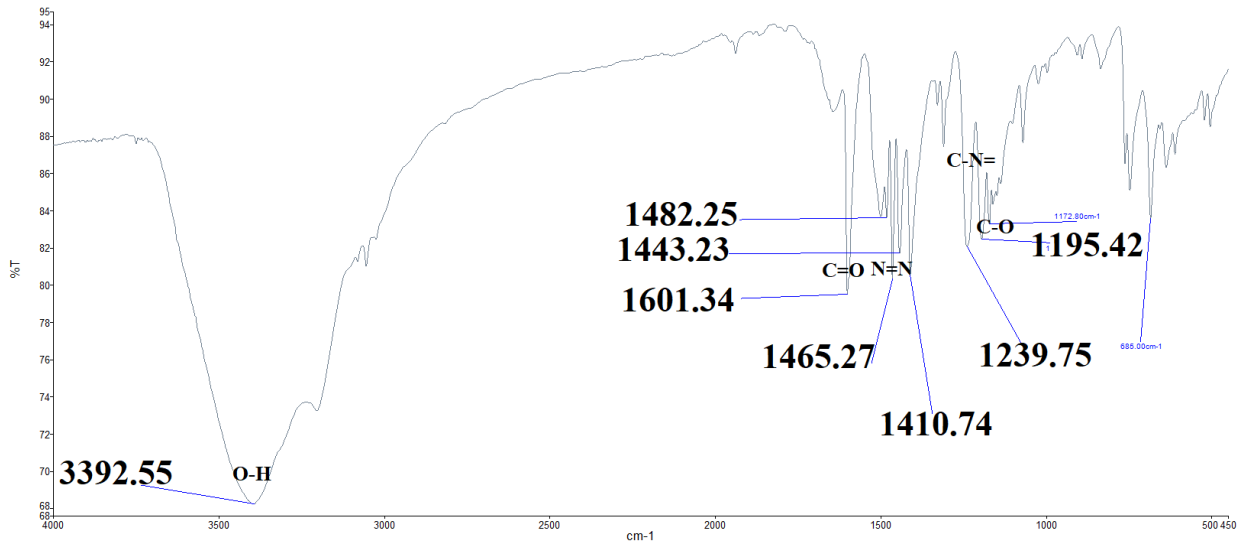

Figure 4.4 IR Spectrum of DYE 4

4.2.5 5-bis(Phenyldiazenyl)-8-hyrdoxyquinoline – Dye 5

Figure 4.5 depicts the IR spectrum of **DYE 5** and displays characteristic frequency regions of the dye. There was an O-H broad ranged from 3600 cm^{-1} to 3150 cm^{-1}. The spectrum below shows an O-H stretch vibration at a peak of 3400 cm^{-1} and a C=N stretch group at1601 cm^{-1}. Also, a N=N stretch for azo bond shows at 1464 cm^{-1} and OH bending for alcohol was detected at 1442 cm^{-1} . A C-N= stretch vibration also shows at 1240 cm^{-1} on the spectrum. The spectrum shows a C-O stretch of tertiary alcohol at 1195 cm^{-1} and aromatic substitution of benzene derivatives at 684cm^{-1}.

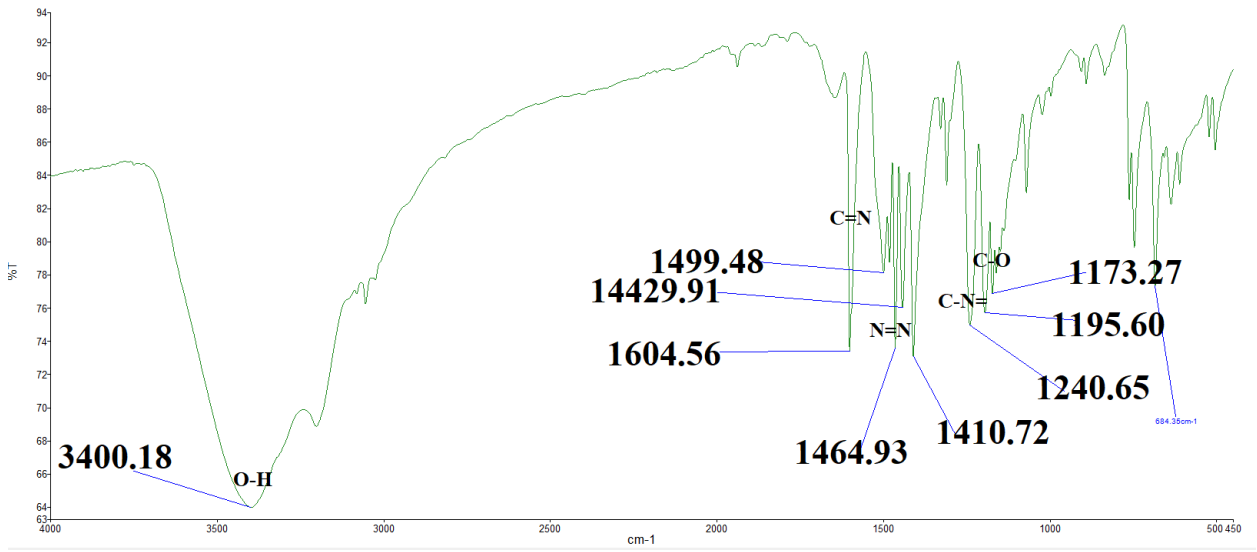

Figure 4.5 IR Spectrum of DYE 5

4.2.6 1-bis(Phenyldiazenyl)-2-naphthalenol – Dye 6

Figure 4.5 depicts the IR spectrum of **DYE 6** and displays characteristic frequency regions of the dye. There was an O-H broad stretch ranged from 3600 cm^{-1} to 3200 cm^{-}. The spectrum below shows an O-H stretch vibration at a high peak of 3398 cm^{-1}. A C=C bond stretch for aromatic was detected at 1601 cm^{-1} and a N=N stretch for azo bond was detected at 1465 cm^{-1}. An O-H bending for alcohol shows at 1411 cm^{-1} and a C-N= stretch vibration was detected at 1242 cm^{-1}. The spectrum shows a C-O stretch of tertiary alcohol at 1200 cm^{-1} and a 1, 2 disubstitution for aromatic derivatives at 784cm^{-1}.

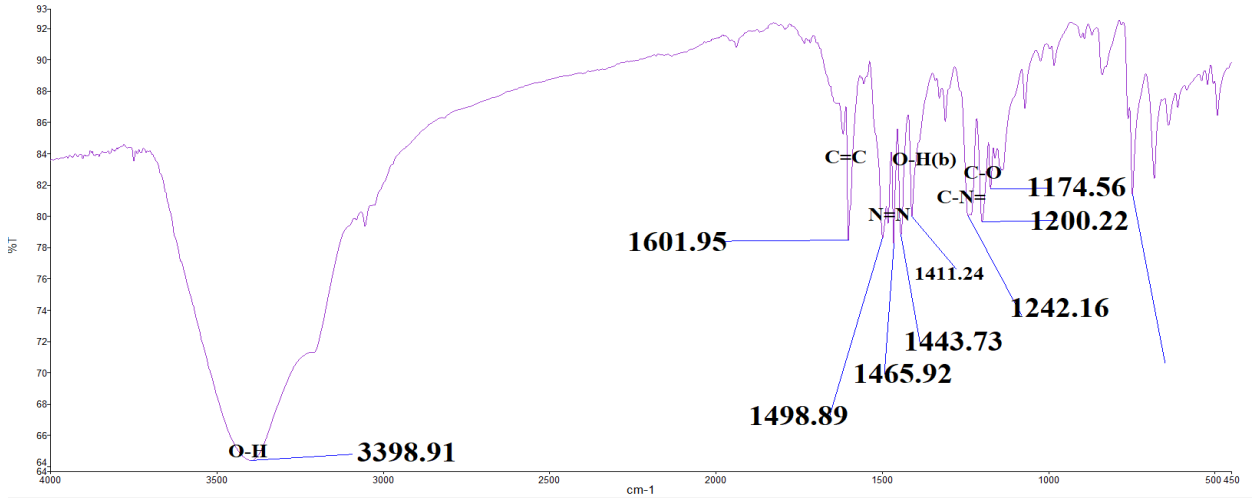

Figure 4.6 IR Spectrum of DYE 6

4.2.7 1-tri(Phenyldiazenyl)sulphanilic acid-2-naphthalenol - DYE 7

Figure 4.7 depicts the IR spectrum of **DYE 7** and displays characteristic frequency regions of the dye. There was an O-H broad stretch ranged from 3550 cm^{-1} to 3200 cm^{-1}. The spectrum below shows a strong peak of O-H stretch vibration at 3392 cm^{-1} and C-N= stretch at 1618 cm^{-1}. A N=N stretch for azo bond was characteristic at 1495 cm^{-1} and an O-H bending for alcohol was detected at 1446 cm^{-1}. Also, a C-O stretch vibration was detected at 1205 cm^{-1} and a S=O stretch for sulphonic acid was shown at 1139 cm^{-1}. A 1, 2 disubstitution for aromatic derivatives was detected at 749cm^{-1}.

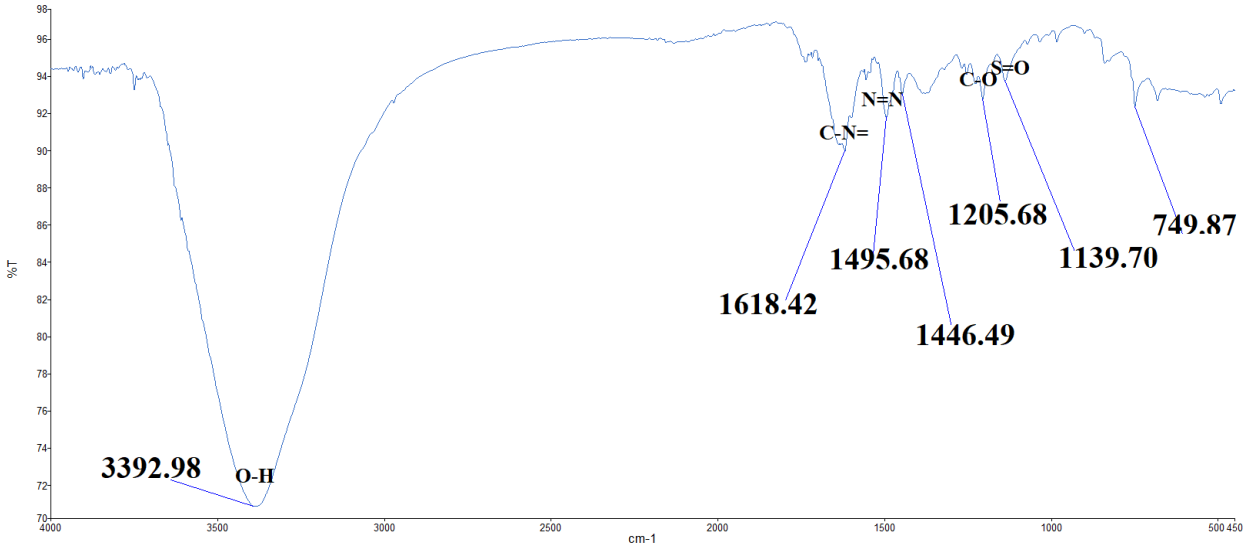

Figure 4.7 IR Spectrum of DYE 7

4.2.8 2-hydroxyl-5-tris (Phenyldiazenylsulphanilic acid)benzoic acid - Dye 8

Figure 4.8 depicts the IR spectrum of **DYE 8** and displays characteristic frequency regions of the dye. There was an O-H broad stretch ranged from 3600 cm^{-1} to 3000 cm^{-1}. The spectrum below shows strong peak of O-H stretch vibration at 3402 cm^{-1}. A C=O stretch group was detected at 1601 cm^{-1} and a N=N stretch for azo bond was detected at 1465 cm^{-1}. An O-H bending for alcohol was detected at 1410 cm^{-1} and a C-O stretch vibration at 1237 cm^{-1}. The spectrum shows a C-N stretch vibration at 1193 cm^{-1} and a S=O stretch for sulphonic acid at 1172 cm^{-1}. A 1, 2, 4 trisubstitution for aromatic derivatives and at 785cm^{-1}indicates.

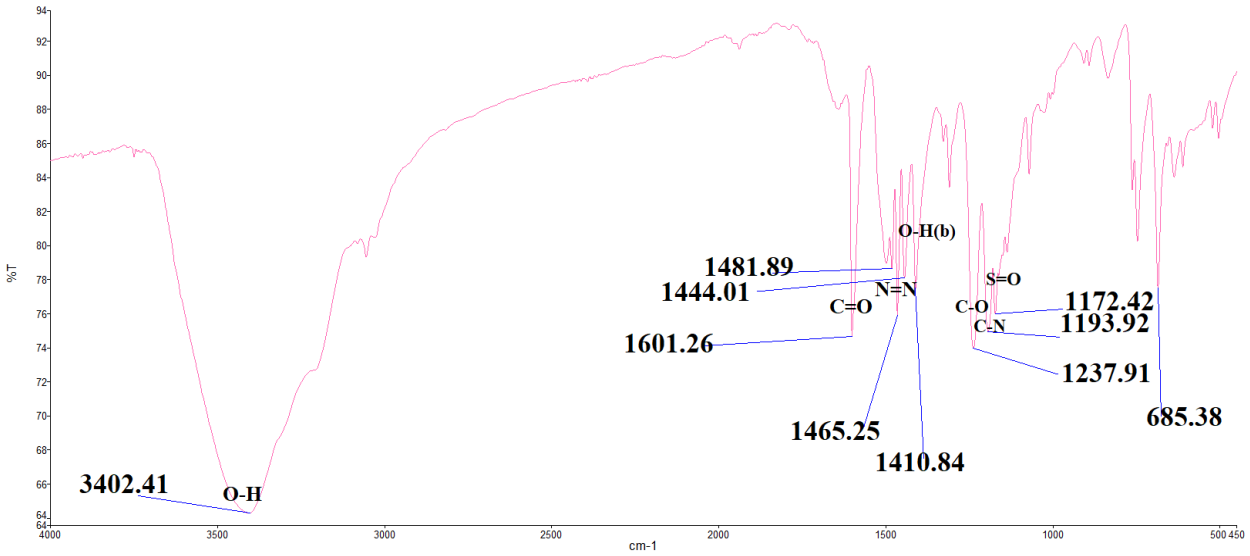

Figure 4.8 IR Spectrum of DYE 8

4.3.1 Nuclear Magnetic Resonance Spectroscopy of DYE 1

^{1}H NMR spectrum of DYE 1

Figure 4.9 depicts the ^{1}H NMR spectrum of **DYE 1** from 1.0 to 8.8 ppm. The spectrum confirms 12 chemically distinct peaks with deuterated chloroform ($CDCl_3$) solvent peak occurring at 7.25 ppm. The O-H proton chemical shifts at positions **c** appear at 4.60 ppm. The aromatic protons of positions a , a^{1}, b, b^{1}, d and d^{1} appear at 8.80 ppm, 8.60 ppm, 8.10 ppm, 8.12 ppm, 7.77 ppm, 7.80 ppm respectively. The other aromatic protons of positions e, e^{1}, f, f^{1}, and g appear at 7.51 ppm, 7.66 ppm, 7.31 ppm, 7.42 ppm and 7.48 ppm respectively.

^{13}C NMR spectrum of DYE 1

Figure 4.10 depicts the ^{13}C NMR spectrum of **DYE 1** from 70.0 to 180.0 ppm. The spectrum confirms 16 chemically distinct peaks with a solvent peaks occurring at 77.26 ppm, 77.01ppm and 76.76ppm. The ^{13}C NMR chemical shifts at positions 1, 2, 3, 4, 5, 6, 7, 8, 9, 10, 11, 12, 13, 14, 15 and 16 appear at 174.50 ppm, 153.20 ppm, 143.23 ppm, 142.04 ppm, 135.45 ppm, 132.63 ppm, 132.07 ppm, 130.91 ppm, 130.19 ppm, 129.78 ppm , 127.71 ppm, 126.89 ppm, 124.00 ppm, 123.09 ppm 118.19 ppm, 114.18 ppm respectively.

The figures below show the ^{1}H NMR and ^{13}C NMR spectra of **DYE 1**

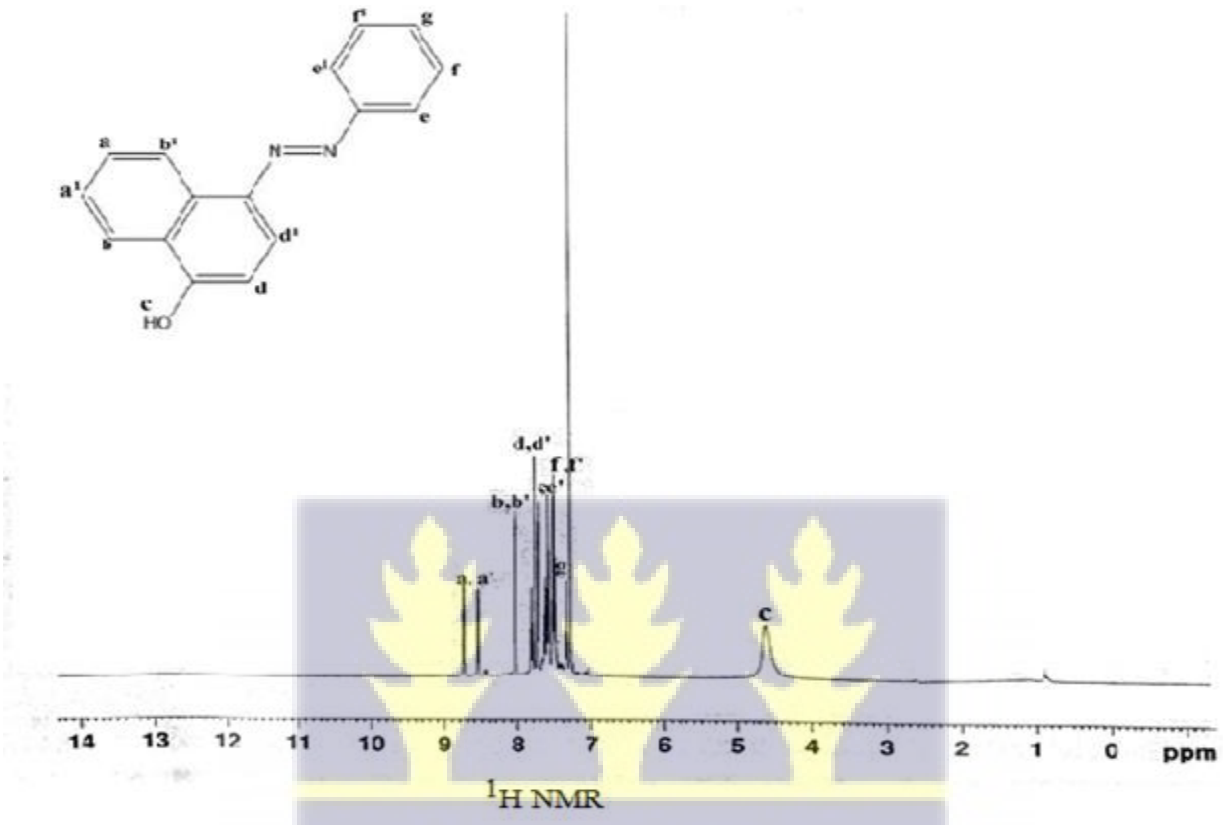

Figure 4.9 ^{1}H NMR Spectrum of DYE 1

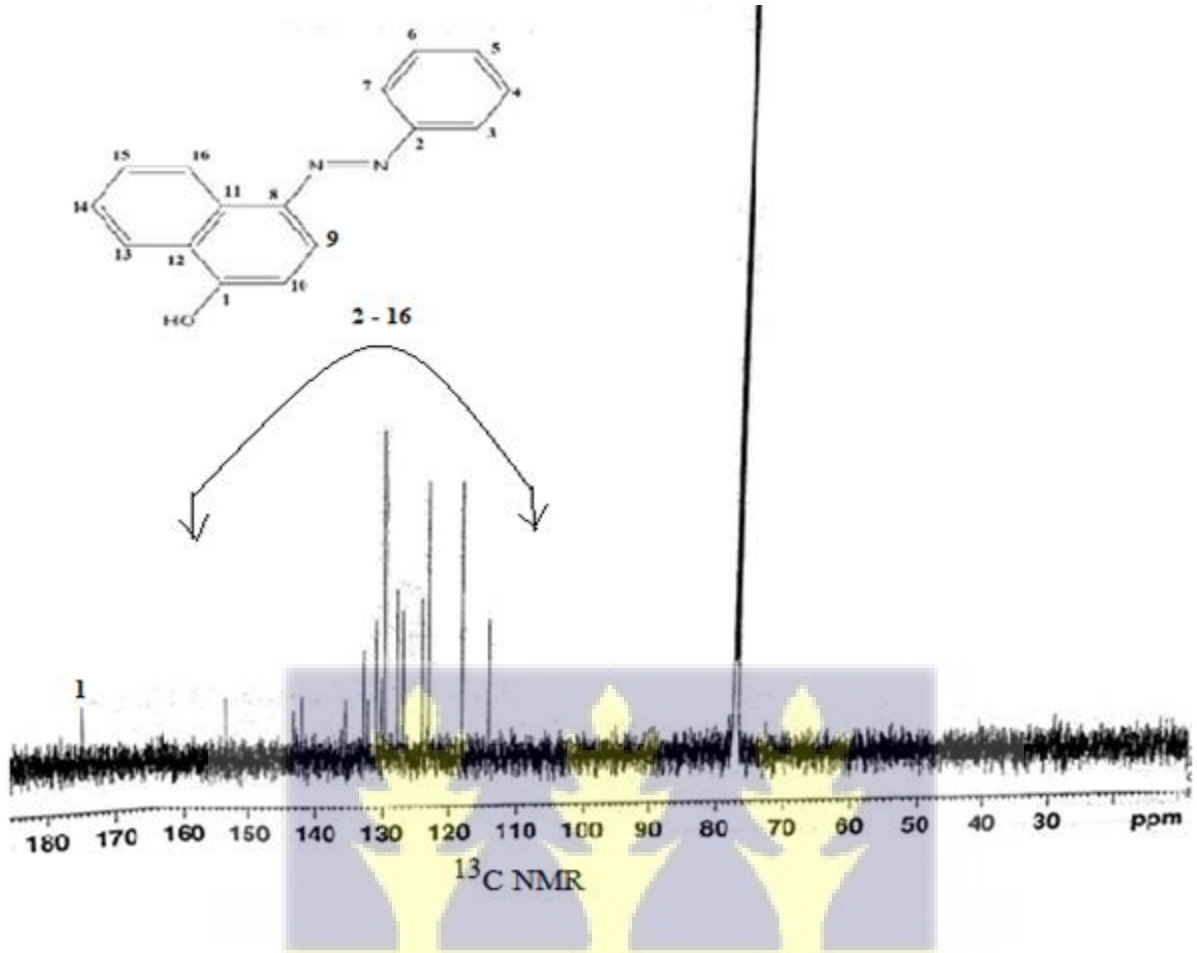

Figure 4.10 ^{13}C NMR Spectrum of DYE 1

4.3.2 Nuclear Magnetic Resonance Spectroscopy of DYE 2

^{1}H NMR spectrum of DYE 2

Figure 4.11 depicts the ^{1}H NMR spectrum of **DYE 2** from 1.0 to 8.8 ppm. The spectrum confirms 12 chemically distinct peaks with a solvent peak occurring at 7.25 ppm. The O-H proton chemical shifts at positions **a** appear at 3.80 ppm. The aromatic protons of positions b, c, d, d^{1}, e and e^{1} appear at 7.82 ppm, 7.83 ppm, 7.78 ppm, 7.72 ppm, 7.70 ppm, 7.68 ppm respectively. The other aromatic protons of positions f, f^{1}, g, g^{1}, and h appear at 7.46 ppm, 7.45 ppm, 7.32 ppm, 7.30 ppm and 8.80 ppm respectively.

^{13}C NMR spectrum of DYE 2

Figure 4.12 depicts the ^{13}C NMR spectrum of **DYE 2** from 70.0 to 180.0 ppm. The spectrum confirms 16 chemically distinct peaks with a solvent peaks occurring at 77.27ppm, 77.01ppm and 76.76ppm.

The ^{13}C NMR chemical shifts at positions 1, 2, 3, 4, 5, 6, 7, 8, 9, 10, 11, 12, 13, 14, 15 and 16 appear at 171.88 ppm, 144.82 ppm, 140.08 ppm, 133.62 ppm, 130.09 ppm, 1129.60 ppm, 129.29 ppm, 128.88 ppm, 128.63 ppm, 118.61 ppm , 127.44 ppm, 125.73 ppm, 124.83 ppm, 121.73 ppm 121.56 ppm, 120.18 ppm respectively.

The figures below show the ^{1}H NMR and ^{13}C NMR spectra of **DYE 2**

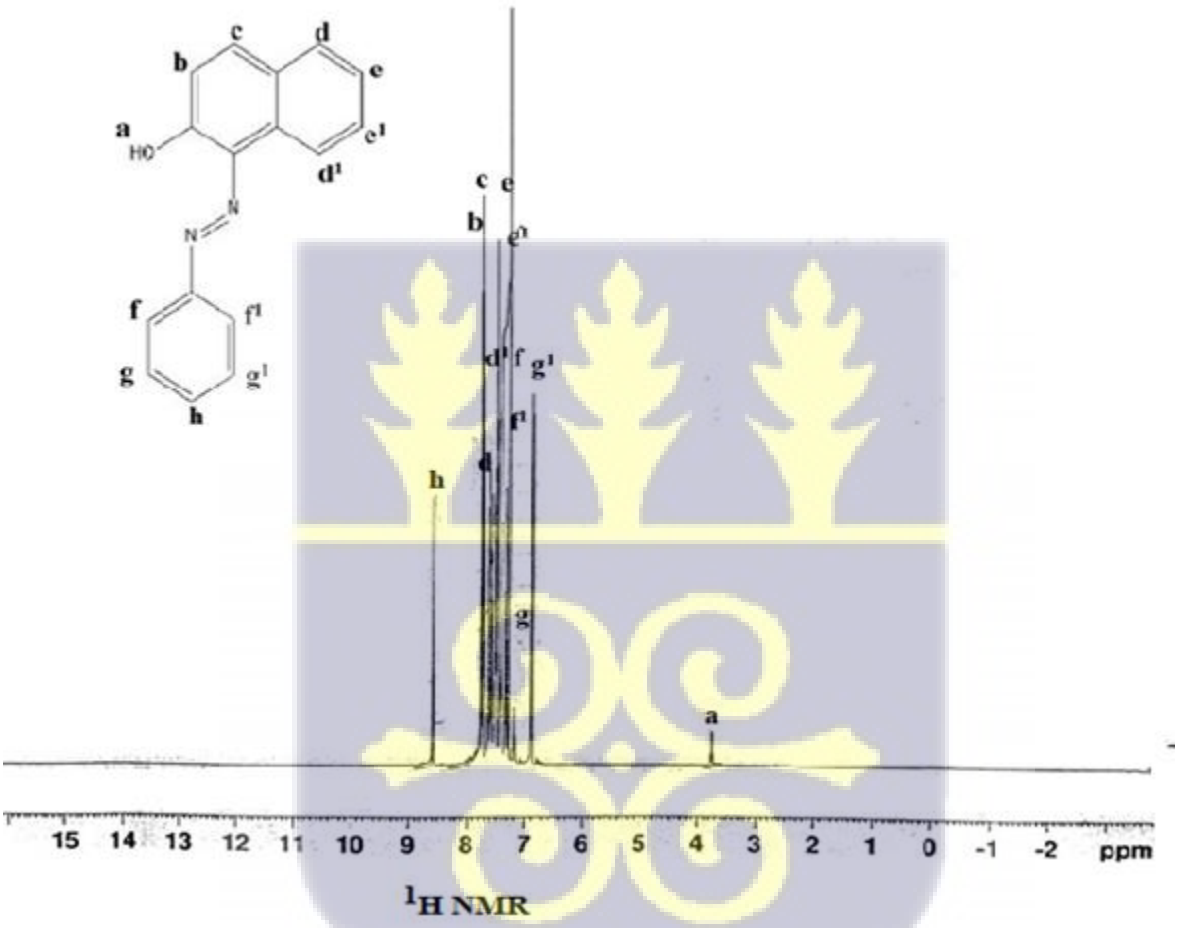

Figure 4.11 ^{1}H NMR Spectrum of DYE 2

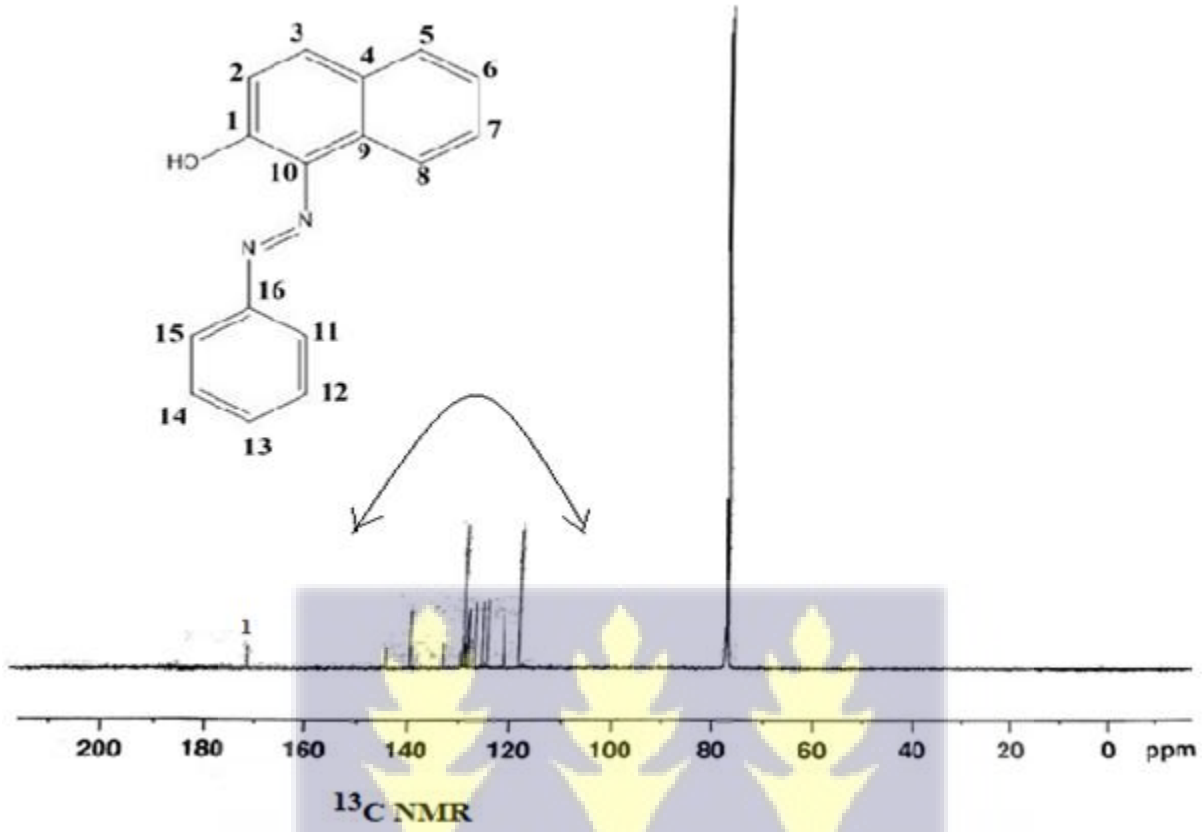

Figure 4.12 ^{13}C NMR Spectrum of DYE 2

4.3.3 Nuclear Magnetic Resonance Spectroscopy of DYE 3

^{1}H NMR spectrum of DYE 3

Figure 4.13 depicts the ^{1}H NMR spectrum of **DYE 3** from 1.0 to 8.8 ppm. The spectrum confirms 11 chemically distinct peaks with a solvent peak occurring at 7.25 ppm. The O-H proton chemical shifts at positions **a** appear at 2.04 ppm. The aromatic protons of positions b, c, d, e, f , g, g^{1}, h, h^{1} and i appear at 9.70 ppm, 9.40 ppm, 9.00 ppm, 8.20 ppm, 8.00 ppm, 7.80 ppm, 7.52ppm, 7.42ppm, 7.12ppm and 7.08ppm respectively. The other aromatic protons of positions f, f^{1}, g, g^{1}, and h appear at 7.46 ppm, 7.45 ppm, 7.32 ppm, 7.30 ppm and 8.80 ppm respectively.

^{13}C NMR spectrum of DYE 3

Figure 4.14 depicts the ^{13}C NMR spectrum of **DYE 3** from 70.0 to 180.0 ppm. The spectrum confirms 15 chemically distinct peaks with a solvent peaks occurring at 77.27ppm, 77.01ppm and 76.76ppm. The ^{13}C NMR chemical shifts at positions 1, 2, 3, 4, 5, 6, 7, 8, 9, 10, 11, 12, 13, 14 and 15 appear at 129.85ppm, 129.53 ppm, 129.34 ppm, 128.83 ppm, 128.00 ppm, 128.03 ppm, 128.14 ppm, 129.10 ppm, 129.14 ppm, 129.08 ppm , 129.04 ppm, 128.91 ppm, 128.94 ppm, 128.54 ppm and 128.14ppm respectively.

The figures below show the ^{1}H NMR and ^{13}C NMR spectra of **DYE 3**

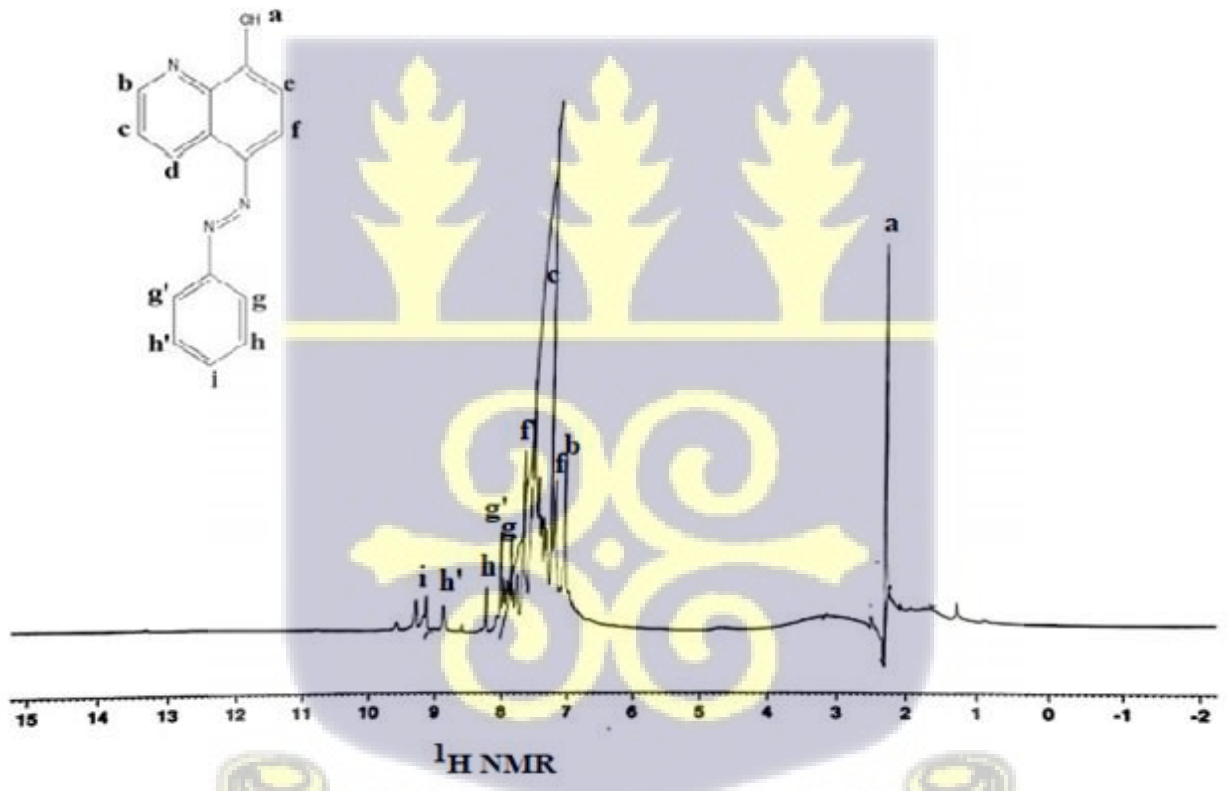

Figure 4.13 ^{1}H NMR Spectrum of DYE 3

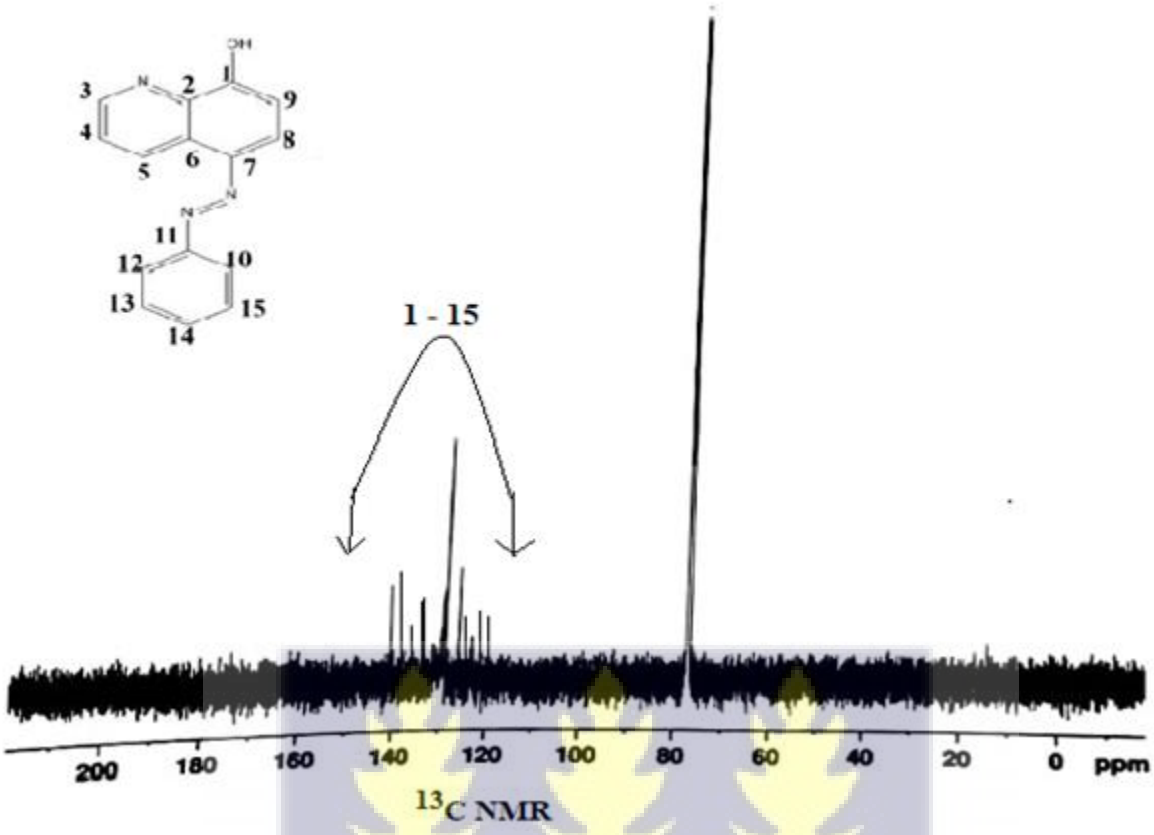

Figure 4.14 ^{13}C NMR Spectrum of DYE 3

4.3.4 Nuclear Magnetic Resonance Spectroscopy of DYE 4

^{1}H NMR spectrum of DYE 4

Figure 4.15 depicts the ^{1}H NMR spectrum of **DYE 4** from 1.0 to 9.6 ppm. The spectrum confirms 14 chemically distinct peaks with a solvent peak occurring at 7.25 ppm. The O-H proton chemical shifts at position **a** appear at 1.80 ppm on an alcohol group. The O-H proton chemical shifts at positions **b** appear at 9.60 ppm on a carboxylic group. The aromatic protons of positions, c, d, e, f, f',g, g',h ,h', i ,i' and j appear at 7.04 ppm, 7.24 ppm, 7.31 ppm, 7.42 ppm, 7.58 ppm, 7.62 ppm 7.66 ppm, 8.02 ppm, 8.08 ppm, 8.10 ppm, 8.14 ppm and 8.16 ppm respectively.

^{13}C NMR spectrum of DYE 4

Figure 4.16 depicts the ^{13}C NMR spectrum of **DYE 4** from 70.0 to 180.0 ppm. The spectrum confirms 19 chemically distinct peaks with a solvent peaks occurring at 77.28ppm, 77.01ppm and 76.76ppm. The ^{13}C NMR chemical shifts at positions 1, 2, 3, 4, 5, 6, 7, 8, 9, 10, 11, 12, 13, 14, 15,16,17,18 and

19 appear at 158.88 ppm for carboxylic group with Hydrogen, 132.82 ppm, 130.08 ppm, 130.02 ppm, 128.10 ppm, 126.60 ppm, 125.29 ppm, 125.18 ppm, 123.60 ppm, 123.56 ppm , 123.44 ppm, 123.23 ppm, 122.83 ppm, 122.73 ppm 122.56 ppm, 121.18 ppm, 121.03 ppm 120.00 ppm, 118.18 ppm respectively.

The figures below show the ^{1}H NMR and ^{13}C NMR spectra of **DYE 4**

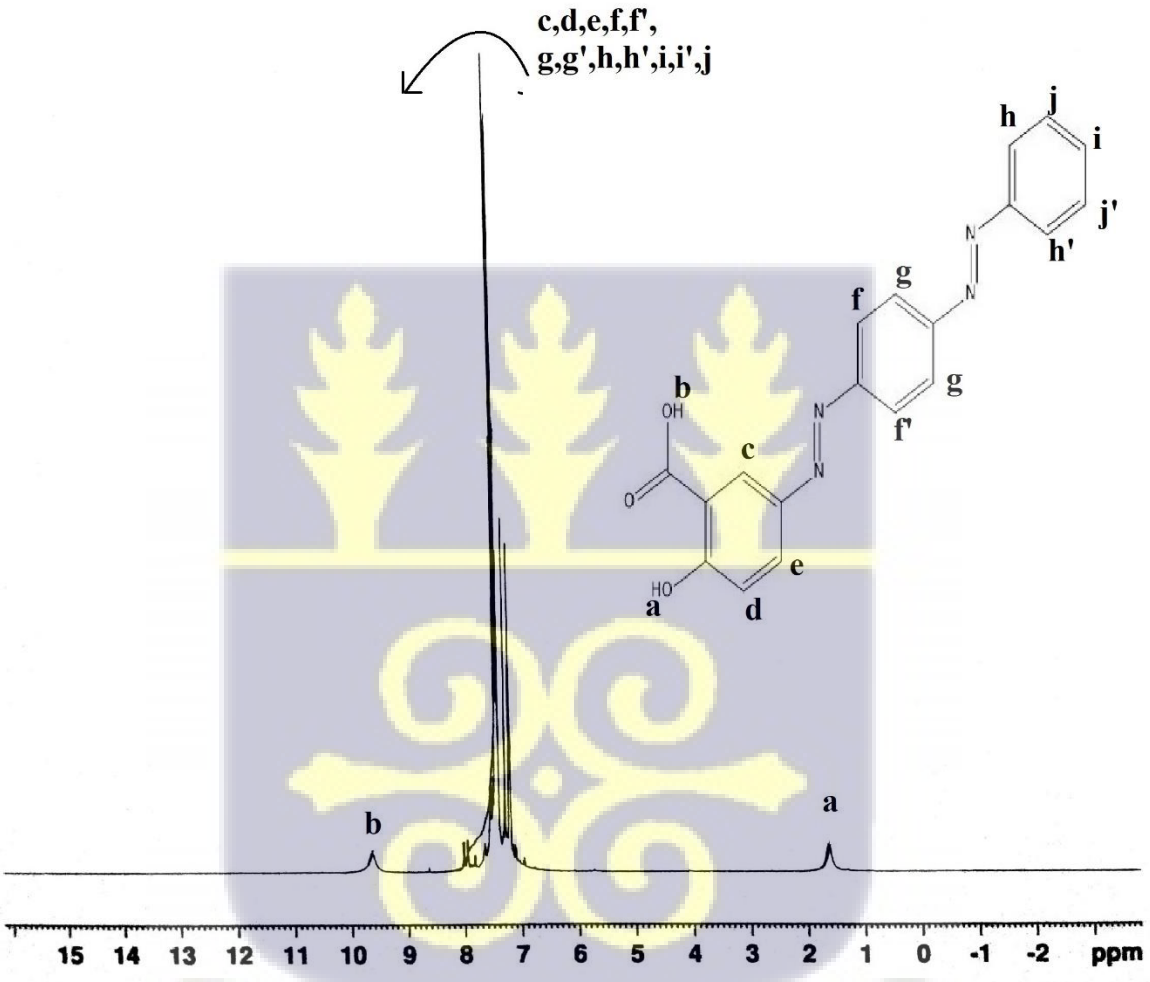

Figure 4.15 ^{1}H NMR Spectrum of DYE 4

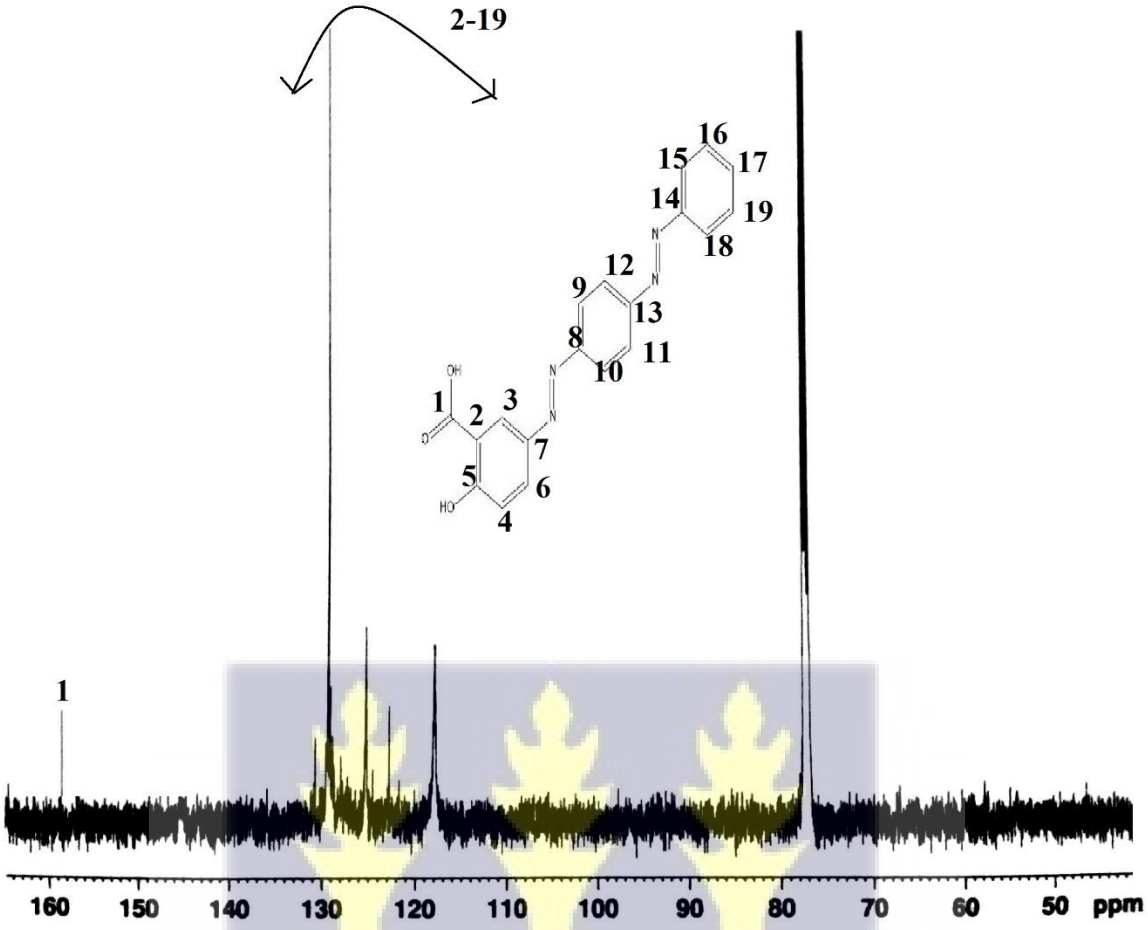

Figure 4.16 ^{13}C NMR Spectrum of DYE 4

4.3.5 Nuclear Magnetic Resonance Spectroscopy of DYE 5

^{1}H NMR spectrum of DYE 5

Figure 4.17 depicts the ^{1}H NMR spectrum of **DYE 5** from 1.0 to 9.6 ppm. The spectrum confirms 14 chemically distinct peaks with a solvent peak occurring at 7.25 ppm. The O-H proton chemical shifts at positions **a** appear at 1.80 ppm on an alcohol group. The O-H proton chemical shifts at positions **b** appear at 9.60 ppm on a carboxylic group. The aromatic protons of positions, c, d, e, f, f',g, g',h ,h', i ,i' and j appear at 7.04 ppm, 7.24 ppm, 7.31 ppm, 7.42 ppm, 7.58 ppm, 7.62 ppm 7.66 ppm, 8.02 ppm, 8.08 ppm, 8.10 ppm, 8.14 ppm and 8.16 ppm respectively.

^{13}C NMR spectrum of DYE 5

Figure 4.18 depicts the ^{13}C NMR spectrum of **DYE 5** from 70.0 to 180.0 ppm. The spectrum confirms 19 chemically distinct peaks with a solvent peaks occurring at 77.28ppm, 77.01ppm and 76.76ppm.

The ^{13}C NMR chemical shifts at positions 1, 2, 3, 4, 5, 6, 7, 8, 9, 10, 11, 12, 13, 14, 15,16,17,18 and 19 appear at 158.88 ppm for carboxylic group with Hydrogen, 132.82 ppm, 130.08 ppm, 130.02 ppm, 128.10 ppm, 126.60 ppm, 125.29 ppm, 125.18 ppm, 123.60 ppm, 123.56 ppm , 123.44 ppm, 123.23 ppm, 122.83 ppm, 122.73 ppm 122.56 ppm, 121.18 ppm, 121.03 ppm 120.00 ppm, 118.18 ppm respectively.

The figures below show the ^{1}H NMR and ^{13}C NMR spectra of **DYE 5**

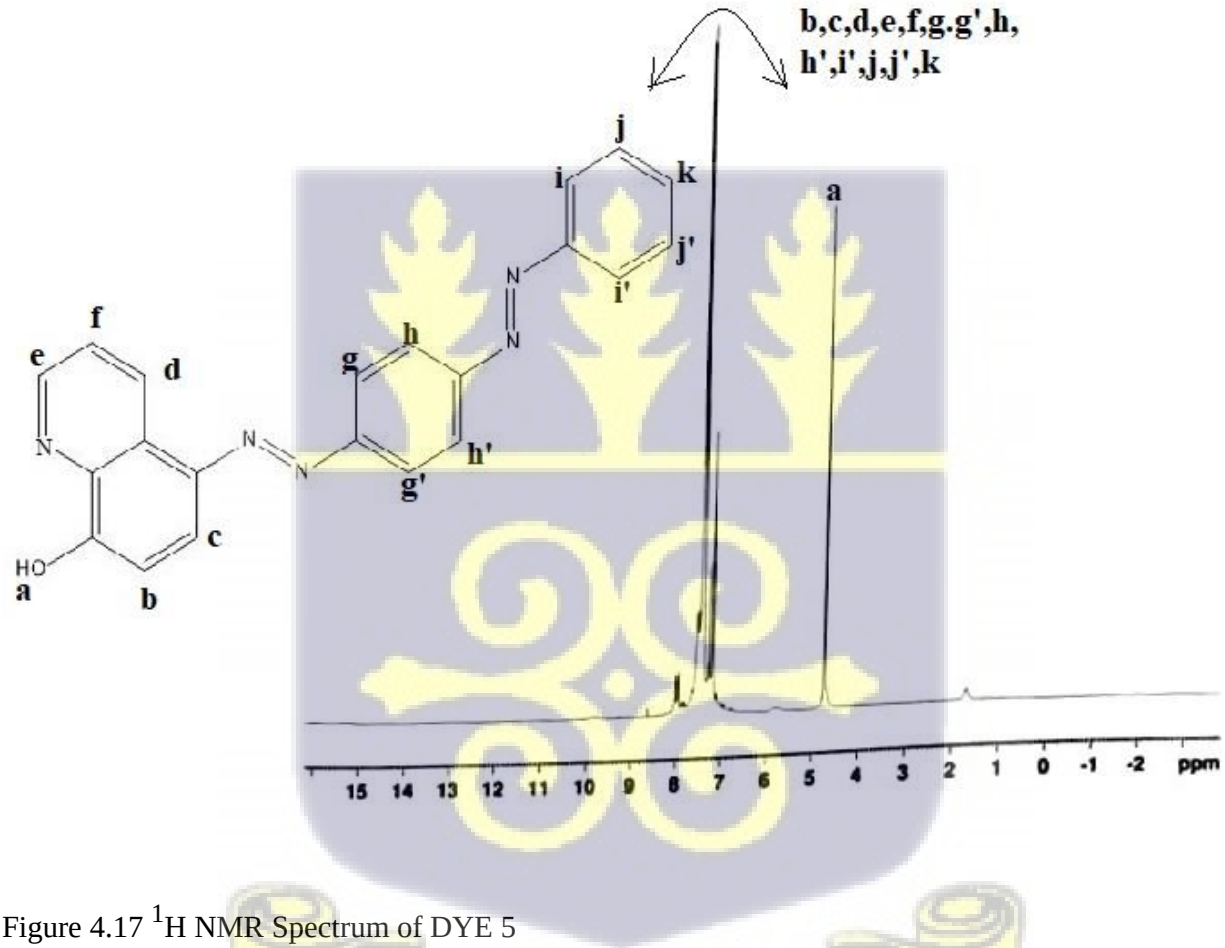

Figure 4.17 ^{1}H NMR Spectrum of DYE 5

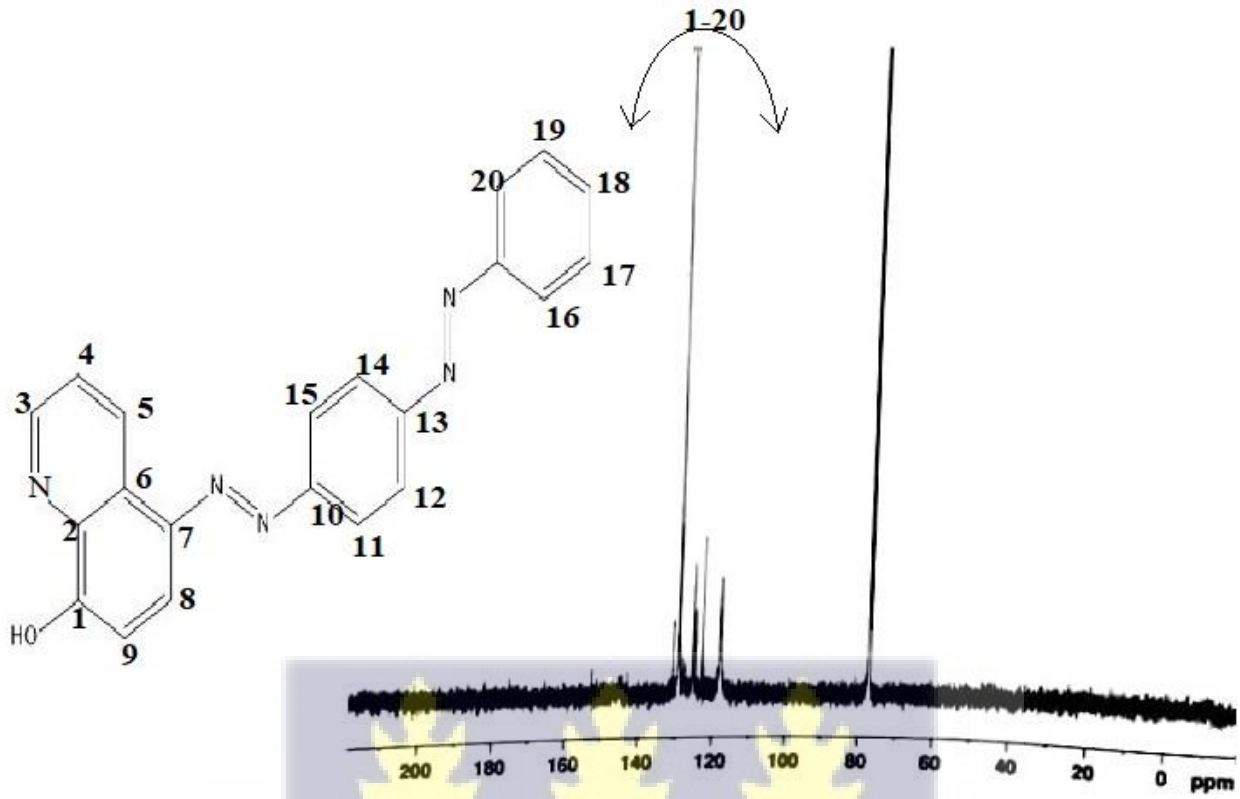

Figure 4.18 ^{13}C NMR Spectrum of DYE 5

4.3.6 Nuclear Magnetic Resonance Spectroscopy of DYE 6

^{1}H NMR spectrum of DYE 6

Figure 4.19 depicts the ^{1}H NMR spectrum of **DYE 6** from 1.0 to 8.8 ppm. The spectrum confirms 16 chemically distinct peaks with a solvent peak occurring at 7.25 ppm. The O-H proton chemical shifts at positions **a** appear at 1.20 ppm on an alcohol group. The aromatic protons of positions, b, c, d, d', e, e', f, f',g, g',h ,h', i ,i'. j. j' appear at 8.80 ppm, 8.44 ppm, 7.92 ppm, 7.82 ppm, 7.78 ppm, 7.70 ppm 7.64 ppm, 7.50 ppm, 7.42 ppm, 7.32 ppm, 7.28 ppm , 7.16 ppm, 7.10 ppm, 7.08 ppm, 7.00 ppm , 6.92 ppm respectively.

^{13}C NMR spectrum of DYE 6

Figure 4.20 depicts the ^{13}C NMR spectrum of **DYE 6** from 70.0 to 180.0 ppm. The spectrum confirms 22 chemically distinct peaks with a solvent peaks occurring at 77.28ppm, 77.01ppm and 76.76ppm. The ^{13}C NMR chemical shifts at positions 1, 2, 3, 4, 5, 6, 7, 8, 9, 10, 11, 12, 13, 14,

15,16,17,18,19,20,21 and 22 appear at 138.88 ppm for carboxylic group with Hydrogen, 131.82 ppm, 131.08 ppm, 130.06 ppm, 128.10 ppm, 127.60 ppm, 127.10 ppm, 125.18 ppm, 123.60 ppm, 123.56 ppm , 123.04 ppm, 122.00ppm, 121.83 ppm, 121.73 ppm 119.56 ppm, 119.16 ppm, 105.03 ppm 103.00 ppm, 102.16 ppm , 118.18 ppm, 107.00 ppm, 104.16 ppm and 97.18 ppm respectively.

The figures below show the ^{1}H NMR and ^{13}C NMR spectra of **DYE 6**

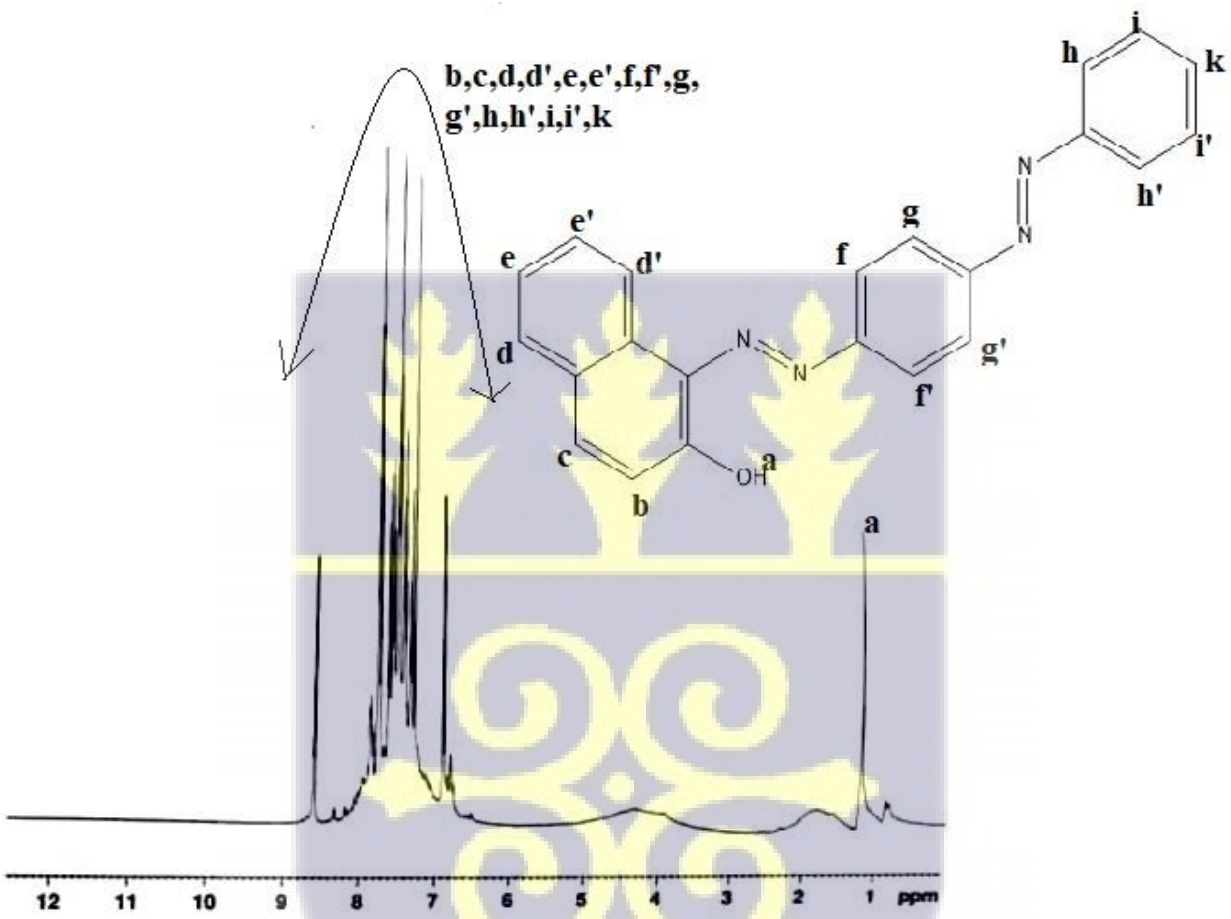

Figure 4.19 ^{1}H NMR Spectrum of DYE 6

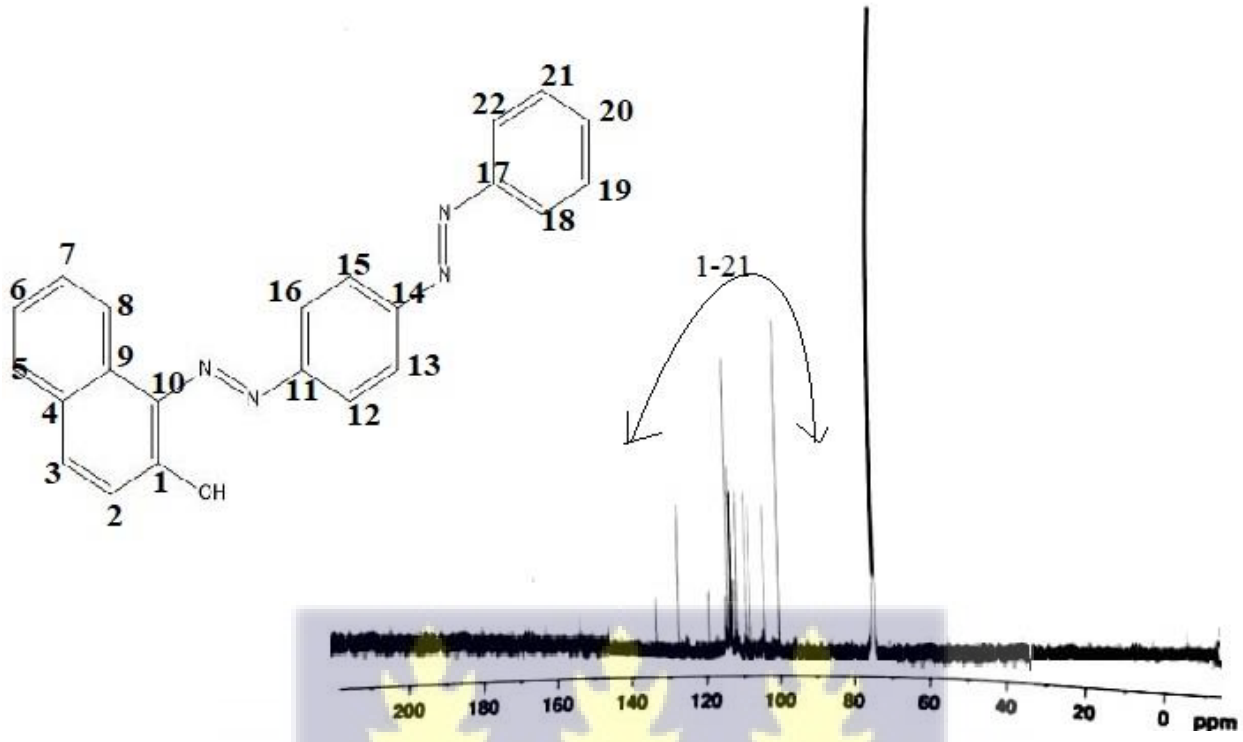

Figure 4.20 ^{13}C NMR Spectrum of DYE 6

4.3.7 Nuclear Magnetic Resonance Spectroscopy of DYE 7

^{1}H NMR spectrum of DYE 7

Figure 4.21 depicts the ^{1}H NMR spectrum of **DYE 7** from 1.0 to 8.8 ppm. The spectrum confirms 20 chemically distinct peaks with a solvent peak occurring at 7.25 ppm. The O-H proton chemical shifts at positions **a** appear at 5.10 ppm. The aromatic protons of positions b , c, d, d, d^{1}, e, e^{1}, f, f^{1},g, g^{1} ,h, h^{1} , i, i^{1}, j, j^{1}, k, k^{1}, l appear at 8.22 ppm, 8.16 ppm, 8.08 ppm, 8.00 ppm, 7.76 ppm 7.70 ppm 7.68 ppm 7.66 ppm 7.66 ppm 7.62 ppm 7.60 ppm 7.60 ppm 7.58 ppm 7.58 ppm 7.54 ppm 7.54 ppm 7.50 ppm 7.50 ppm 8.42 ppm respectively.

^{13}C NMR spectrum of DYE 7

Figure 4.22 depicts the ^{13}C NMR spectrum of **DYE 7** from 70.0 to 180.0 ppm. The spectrum confirms 28 chemically distinct peaks with a solvent peaks occurring at 77.26 ppm, 77.01ppm and 76.76ppm. The ^{13}C NMR chemical shifts at positions 1, 2, 3, 4, 5, 6, 7, 8, 9, 10, 11, 12, 13, 14,

15,16,17,19,20,21,22,23,24,25,26,27 appear within 110 to 146. A chemical shift for 28 appears at 172ppm

The figures below show the ^{1}H NMR and ^{13}C NMR spectra of **DYE 7**

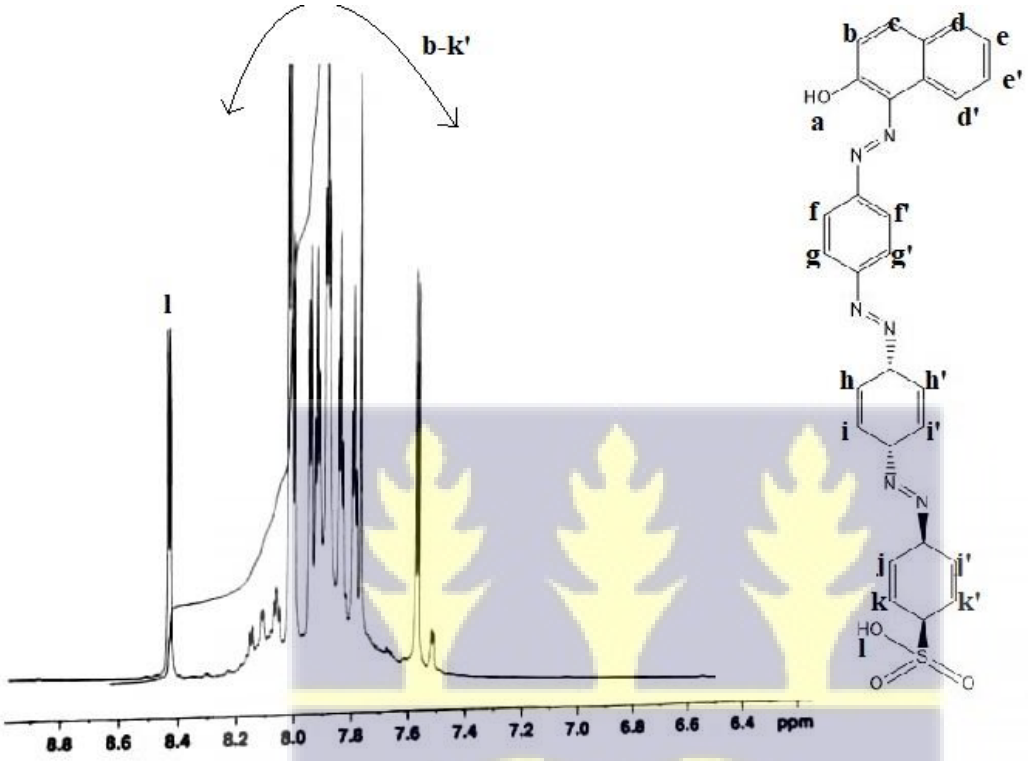

Figure 4.21 ^{1}H NMR Spectrum of DYE 7

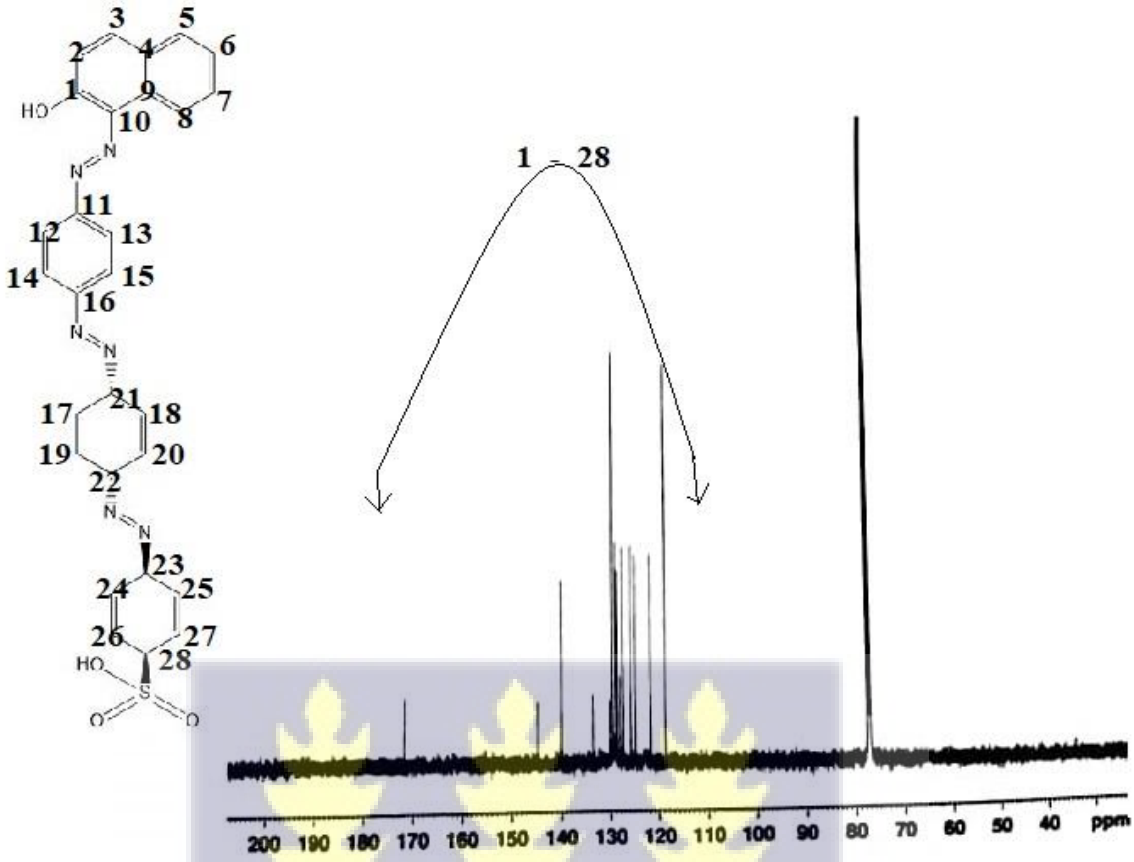

Figure 4.22 ^{13}C NMR Spectrum of DYE 7

4.3.8 Nuclear Magnetic Resonance Spectroscopy of DYE 8

^{1}H NMR spectrum of DYE 8

Figure 4.23 depicts the ^{1}H NMR spectrum of **DYE 8** from 1.0 to 8.8 ppm. The spectrum confirms 18 chemically distinct peaks with a solvent peak occurring at 7.25 ppm. The O-H proton chemical shifts at positions **a** appear at 1.20 ppm on an alcohol group. The aromatic protons of positions b, b', c, c', e, e',f, f',g ,g', h, i , j, k, l appear at 8.10 ppm, 8.02 ppm, 7.82 ppm, 7.80 ppm, 7.78 ppm, 7.70 ppm 7.64 ppm, 7.480 ppm, 7.40 ppm, 7.30 ppm, 7.18 ppm , 7.12 ppm, 7.08 ppm, 7.06 ppm, 7.00 ppm , 6.92 ppm respectively.

^{13}C NMR spectrum of DYE 8

Figure 4.24 depicts the ^{13}C NMR spectrum of **DYE 8** from 70.0 to 180.0 ppm. The spectrum confirms 25 chemically distinct peaks with a solvent peaks occurring at 77.28ppm, 77.01ppm and 76.76ppm. The ^{13}C NMR chemical shifts at positions 1, 2, 3, 4, 5, 6, 7, 8, 9, 10, 11, 12, 13, 14,

15,16,17,18,19,20,21, 22, 23, 24 and 25 appear at 138.88 ppm for carboxylic group with Hydrogen, 130.82 ppm, 130.08 ppm, 130.04 ppm, 130.00 ppm, 129.60 ppm, 129.10 ppm, 129.08 ppm, 128.60 ppm, 128.56 ppm , 128.04 ppm, 128.00ppm, 126.83 ppm, 126.73 ppm 124.56 ppm, 122.16 ppm, 121.03 ppm 125.00 ppm, 123.16 ppm , 122.18 ppm, 122.00 ppm, 118.16 ppm and 118.10 ppm, 120.10 ppm, 112.16 ppm and 142.12 ppm respectively.

The figures below show the ^{1}H NMR and ^{13}C NMR spectra of **DYE 8**

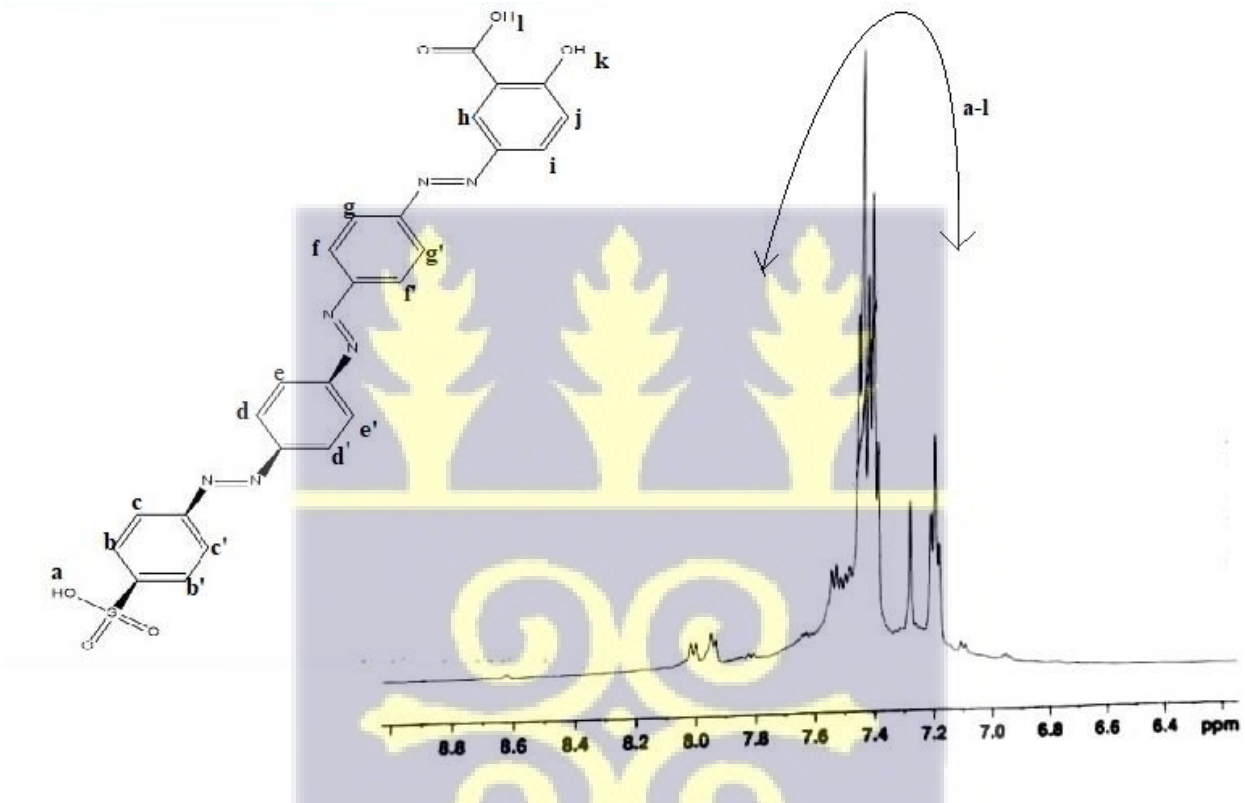

Figure 4.23 ^{1}H NMR Spectrum of DYE 8

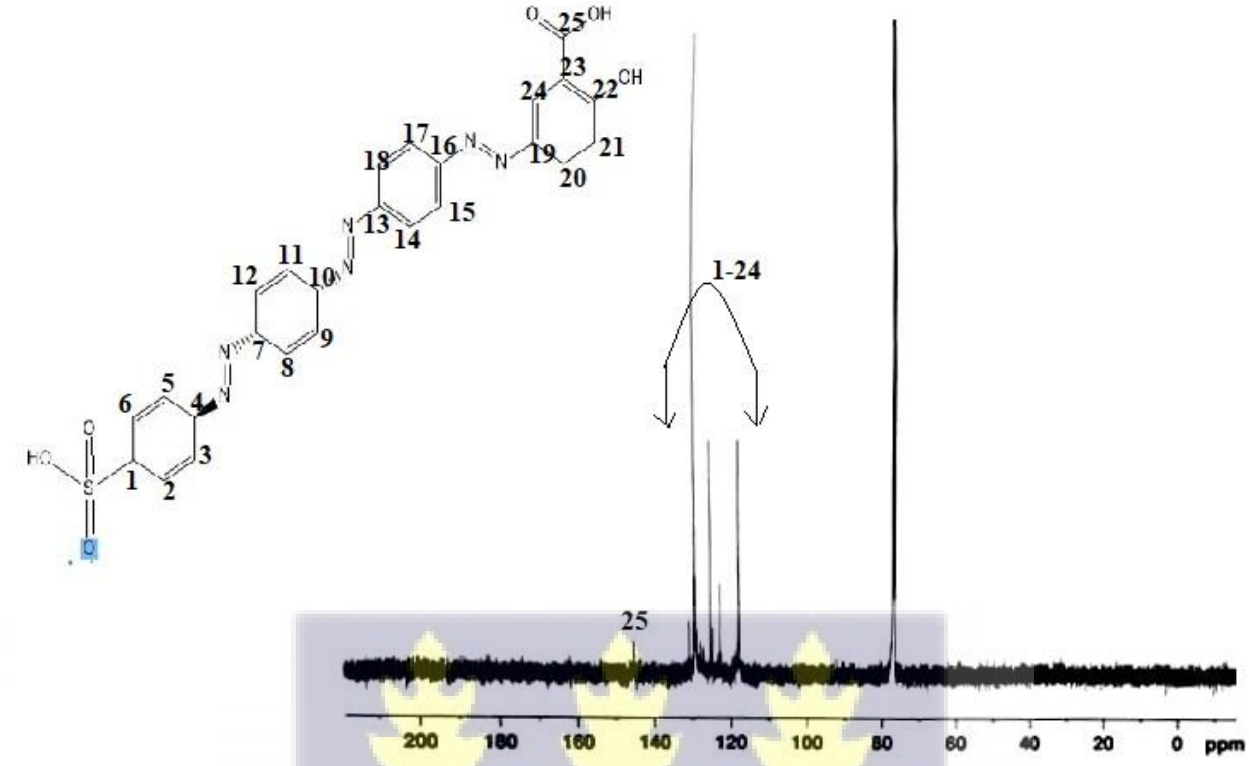

Figure 4.24 ^{13}C NMR Spectrum of DYE 8

4.4 UV-Vis Absorption spectra of Dyes

When a material absorbs light in the ultraviolet and visible region, electrons are promoted from lower energy level to the higher excited state, as stated in molecular orbital theory. The spectrum of the **DYE 1** (Figure 4.25) shows a broad spectral absorption between 250 nm to 650 nm with three absorption maxima at 291 nm, 355.5 nm and 518 nm. The wavelength 355.5 nm is as a result of π - π * molecular electronic transition. The wavelength 518nm is as result of the **n to π*** transition matches with electron excitation from one of the unshared pair to the **π*** orbital (Kunkely & Vogler, 2001). The locations of the absorption maxima and the nature of the spectrum is characteristic of conjugated system of π electrons. The spectrum of the **DYE 2** (Figure 4.25) shows a broad spectral absorption between 250 to 567 nm with two absorption maxima at 360 nm and 478nm. These absorption peaks may be due to π-π* and n-π* respectively of the azo group (Silverstein, Bassler & Morrill, 1981; Kumar, Mahiya & Mathur , 2011). The locations of the absorption

maxima and the nature of the spectrum is characteristic of conjugated system of π. The spectrum of the **DYE 3** (Figure 4.25) shows a broad spectral absorption between 260 nm to 580 nm with one absorption maxima at 352 nm. The spectrum of the **DYE 4** (Figure 4.25) shows a broad spectral absorption between 280 nm to 550 nm with one absorption maximum at 353.5 nm. The locations of the absorption maxima and the nature of the spectrum is characteristic of conjugated system of π electrons. Structurally, azodyes have a conjugated system, in which the π electrons are highly delocalized. This causes a reduction in the HOMO – LUMO energy gap making the excited state to have reduced energy value. The energy therefore required to bring about the π - π * molecular electronic transition becomes smaller and matches with light in the visible region, explaining why **DYE 1** and **2,** absorbs light in the visible region (Scotter, 2009). **DYE 3** and **DYE 4** match absorption in the UV region.

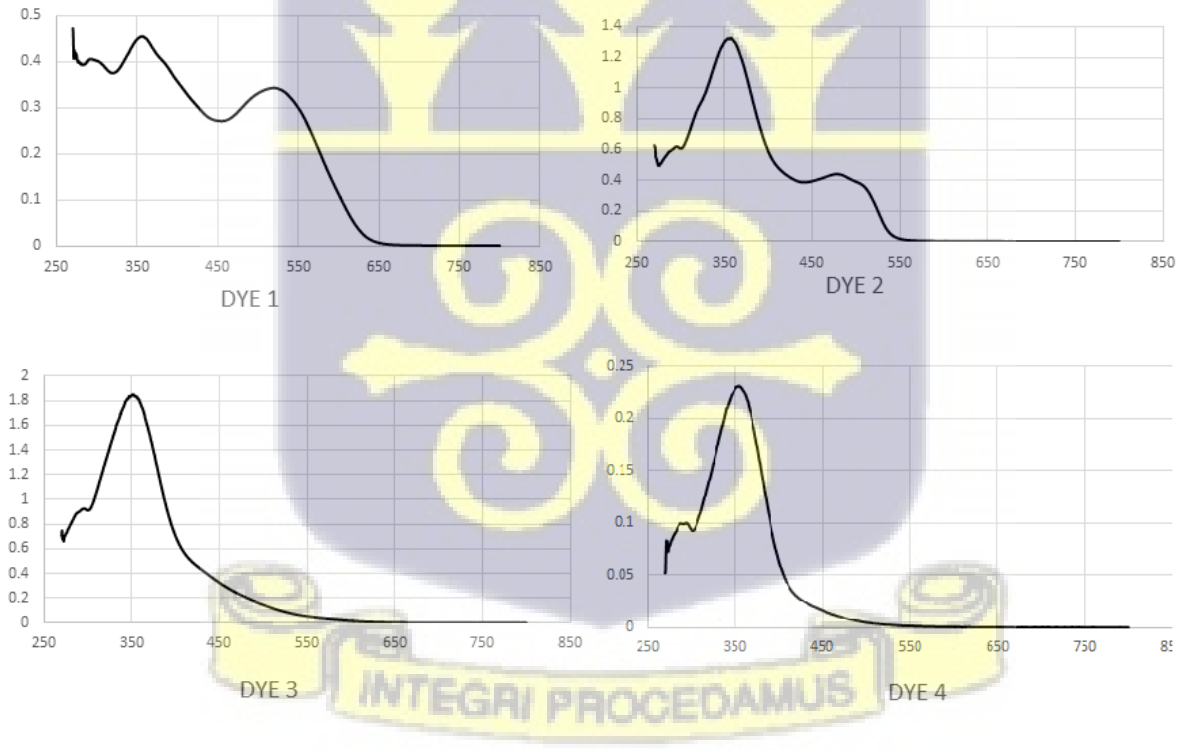

Figure 4.25 UV spectrum of Dye 1, 2, 3 and 4

The spectrum of the **DYE 5** (Figure 4.26) shows a broad spectral absorption between 250 nm to 550 nm with an absorption maxima at 355 nm. The spectrum of the **DYE 6** (Figure 4.26) shows a broad spectral absorption between 280 nm to 600 nm with two absorption maxima at 480 nm

and 354 nm. The locations of the absorption maxima and the nature of the spectrum is characteristic of conjugated system of π electrons. The spectrum of the **DYE 7** (Figure 4.26) shows a broad spectral absorption between 250 nm to 600 nm with three absorption maxima at 315 nm, 392 nm, 469 nm. According to a study to determine absorption spectra of the azo dyes, different solvents were used and it exhibited maximum absorption band in the range of 300 to 438 nm which was attributed to the **π - π *** molecular electronic transition transitions of azo -N=N-group (Mallikarjuna & Keshavayya, 2020). Again, according to Kunkely and Vogler (2001) the **n to π*** transition matches with excitation of an electron from one of the unshared pair to the **π*** orbital which occur close to 500 nm. The spectrum of the **DYE 8** (Figure 4.26) shows a broad spectral absorption between 250 nm to 520 nm with two absorption maxima at 294 nm and 353 nm. The locations of the absorption maxima and the nature of the spectrum is characteristic of conjugated system of π electrons. This absorption is attributed to a π - π * molecular electronic transition.

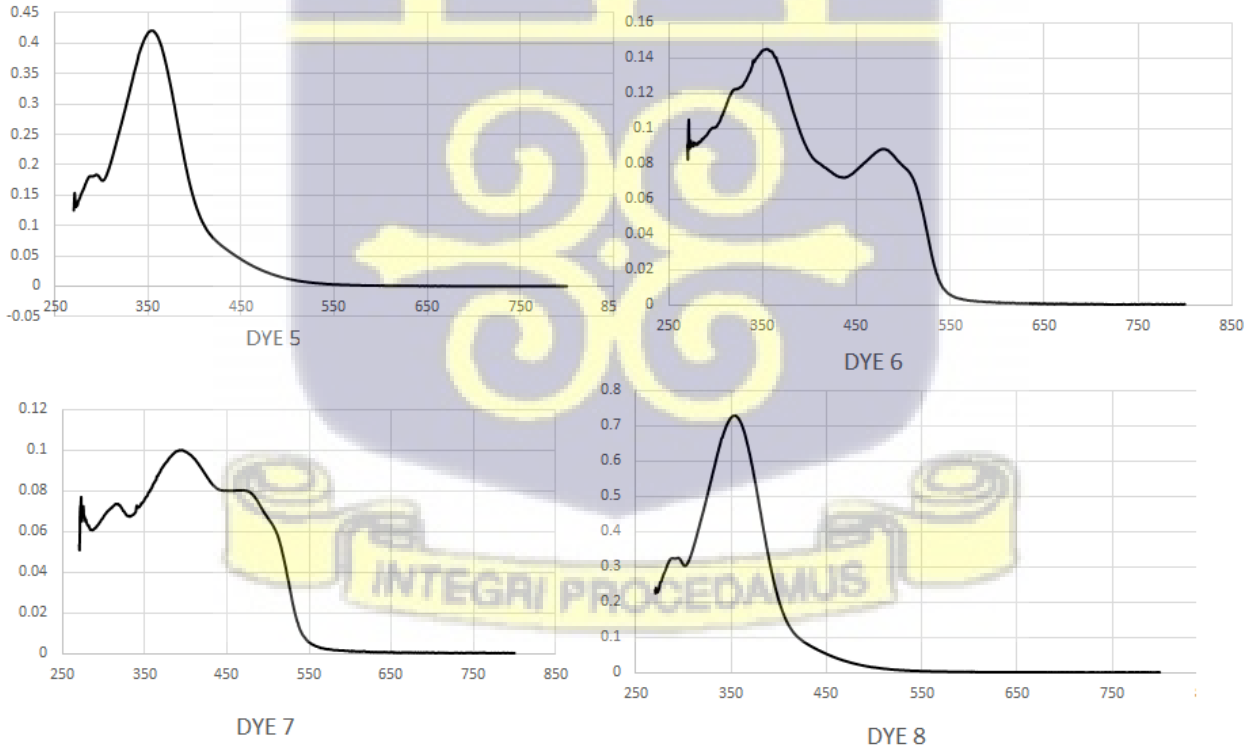

Figure 4.26 UV-VIS spectrum of Dye 5, 6, 7 and 8

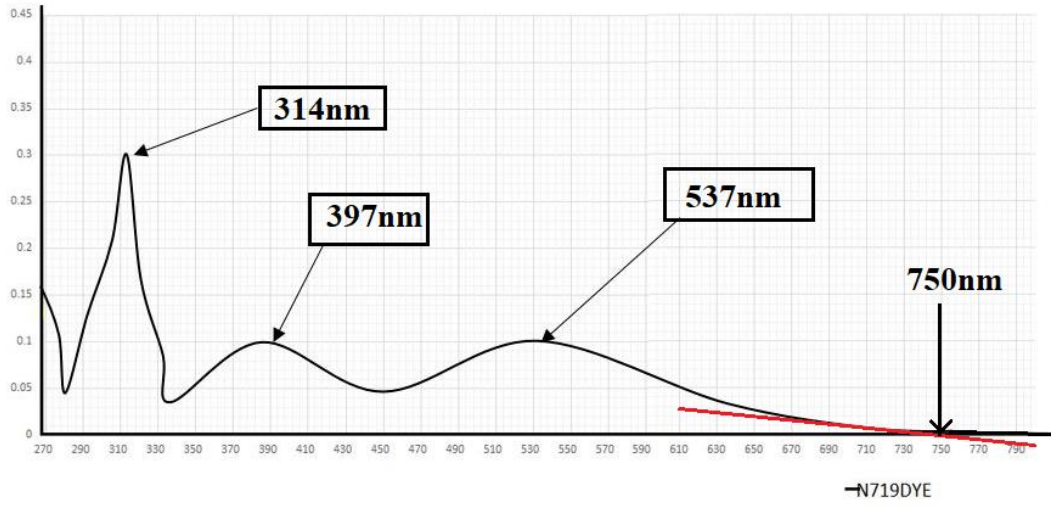

Figure 4.27 UV-VIS spectrum of N719 dye

The spectrum of the standard **N719** dye **(Figure 4.27**) showed a broad spectral absorption ranging from 250 nm to 800 nm with three absorption maxima. There are two visible absorption bands at 535 nm and 397 nm as well as a UV absorption band at 314 nm. The former two absorption bands are ascribed to metal-to-ligand charge transfer transitions while the last is ascribed to intra-ligand (π - π *) charge-transfer transition (Giovannetti, 2012).

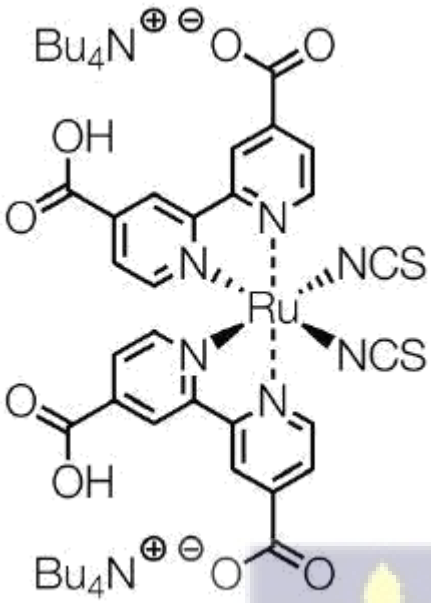

Figure 4.28 Structure of N719 dye

From **Figure 4.29**, it is observed that in terms of broader absorptions in the visible region (350 nm – 800 nm), **DYE 1, 2, 6 and 7** compares closely to the standard **N719** followed by **DYE 3, 4, 5** and **8** least absorption. Based on this observation, **DYE 1, 2, 6 and 7** should harvest a lot of incident photons as possible in the visible region and hence are good sensitizer candidates for DSSCs application. **DYE 3, 4, 5** and **8** on the other hand, are not good candidate because of the poor absorption it exhibits in the visible region from 400 nm to 800 nm (**Figure 4.29**).

4.5 Optical Bandgap

According to Burrows et al (2006), the optical band gap which is the difference between HOMO and LUMO levels, can be calculated using the onset of absorption from the longest wavelength absorption edges (λonset) in the UV-Vis absorption spectra. The onset value is the intersection of the extrapolations of the linear parts of the spectrum relating to the wavelength as shown in **Figure 4.29**. The optical band gaps (E_g) were calculated using the equation 4.1 below:

$$\mathbf{Eg} = h \times f = \frac{h \times c}{\lambda onset} = \frac{1241}{\lambda \mathbf{onset}} \qquad \mathbf{4.1}$$

Where: h is Planck's constant;

c is the speed of light and

λ_{onset} is onset of absorption from the longest wavelength absorption edges in nm.

E_g optical band gap energy

Table 4.2: Maximum absorption peaks (λ_{max}), onset of absorption from the longest wavelength absorption edges (λ_{onset}) and calculated optical band gap (E_g) for DYE 1,2,3,4,5,6,7,8 and N719 dye.

Compound	λmax (nm)	λonset (nm)	Eg (eV)
DYE 1,	291, 355.5, 518	630	1.969
DYE 2	360, 478	540	2.29
DYE 3	352	430	2.886
DYE 4	353.5	430	2.886
DYE 5	355	433	2.866
DYE 6	480, 354	544	2.281
DYE 7	315, 392, 469	550	2.256
DYE 8	294 ,353	430	2.886
N719 DYE	314, 397, 535	750	1.65

The optical band gaps (Eg) of dyes (1, 2, 3, 4, 5, 6, 7 and 8), in **Table 4.2** correspond to energy in the visible region in the electromagnetic spectrum. The smaller the Eg value of a dye molecule, the greater the number of photons they can harvested in the visible region and the better the efficiency of the device. Hence, based on their Eg values, **DYE 1** is expected to absorb more photon than **DYE 2, 6 and 7**. The Eg values of **DYE 3, DYE 4**, **DYE 5 and DYE 8** are 2.886, 2886, 2.866 and 2.886 respectively. **DYE 5** on the other hand is also expected to absorb more photons than **DYE 3, 4 and 8**. The small Eg of **DYE 1** and **DYE 2, 6 and 7** suggests that the

distances between their HOMO and LUMO levels is such that the energy in the visible region is enough to cause electron promotion from their valence band into their conduction band.

DYE 3, 4 and 8 on the other hand, have relatively high Eg of 2.886 eV respectively which is almost close to that of the semiconductor (TiO_2 -3.2 eV) (Sboui etal, 2021). This implies that more energy is needed to move electrons from the valence band region into the conduction band region and corresponds to energy in the UV region.

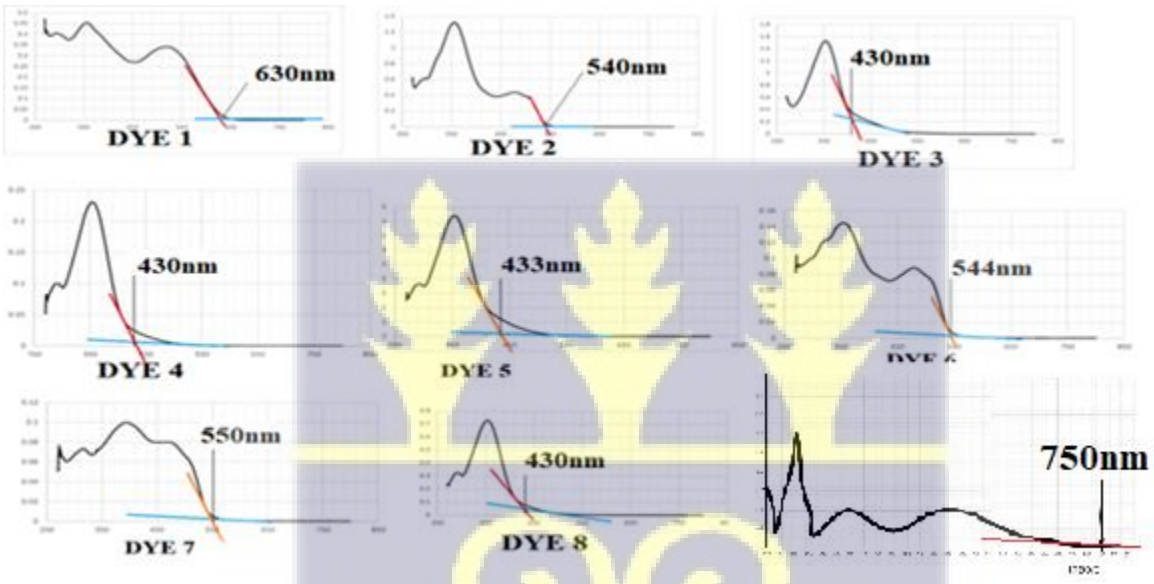

Figure 4.29 longest wavelength absorption edges (λ_{onset}) for dye 1, 2, 3, 4, 5, 6, 7, 8 and N719dye

4.5 Electrochemical Properties

Electrochemical properties of the synthesized dyes were analysed using cyclic voltammetry to study the **DYES** (**Figure 4.8** represents their voltammograms).The measurements were used to determine the HOMO values of the DYES. CV is a potentiodynamic electrochemical measurement. CV is measured with a three electrode arrangement (with three-electrode electrochemical cell) whereby the potential relative to some reference electrode is scanned at a working electrode while the resulting current flowing through a counter (or auxiliary) electrode is monitored in a quiescent solution (Petrova et al, 2013). The LUMO energy level of the dyes were calculated according to

equation 4.3, using E_g values calculated from UV-Vis absorption spectrum (Petrova et al, 2013). The HOMO level characterizes the energy needed to remove an excited electron in a molecule, this is described as oxidation process. The LUMO level is the energy required to inject an electron into a molecule, this is a reduction process (**Figure 4.30**). According to Pommerehene etal (1995), Ferrocene was used in their experiment as the known reference standard to calculate the HOMO and LUMO levels. The energy levels of the DYES were calculated using the oxidation onset (E_{ox}) values obtained from CV curves as shown in **Figure 4.30** and computed using the empirical relations including the ferrocene value of -4.8 eV (as cited by Antwi et al, 2016).

HOMO = [-4.8 - E_{ox}] eV **4.2**

LUMO = [HOMO + E_g] eV **4.3**

Where E_{ox} is the onset oxidation potentials of the compounds; and E_g is optical band gap energy of the compounds determined from UV-vis spectra.

All CV measurements were referenced to ferrocene and compared with that of the standard N719 dye.

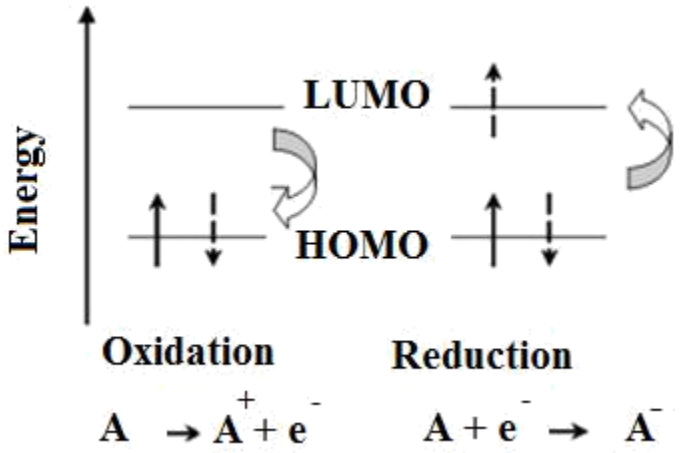

Figure 4.30: Diagram showing that the oxidation and reduction of molecules involve electron transfers.

As shown in Figure 4.31, **DYE 1** and **DYE 2** exhibit oxidation and reduction processes. **DYE 1** and **DYE 2** exhibits an oxidation process with no oxidation peak observed at from their respective voltammograms. The standard **N719** dye exhibited a reversible redox process with an oxidation peak at +0.75 V.

The onset oxidation potentials of the compounds were determined from the corresponding tangent lines of the CV curves shown in Figure 4.32. The values were 0.28V, 0.30V, 0.60V, 0.56V, 0.52V, 0.63V, 0.66V and 0.60V for **DYE 1, DYE 2, DYE 3, DYE 4, DYE 5, DYE 6, DYE 7** and **DYE 8** respectively. The standard **N719** dye had the highest onset oxidation potential of 0.55 V.

The HOMO and LUMO levels of the compounds were calculated according to equation 4.2, and 4.3 respectively. The HOMO levels for **DYE 1, DYE 2, DYE 3, DYE 4, DYE 5, DYE 6, DYE 7** and **DYE 8** were determined to be -5.08 eV, -5.10 eV, -5.40 eV, -5.36 eV, -5.36 eV, -5.43 eV, -5.46 eV and -5.40 eV respectively. The calculated HOMO level of the standard **N719** dye is -5.35 eV(Solaronix, 2013), which is lower in energy than **DYE 1** and **DYE 2** but greater in energy than **DYE 3, DYE 4, DYE 5, DYE 6, DYE 7** and **DYE 8.** The LUMO levels were estimated as -3.11 eV for **DYE 1**; -2.81 eV for **DYE 2;** -2.514 eV for **DYE 3;** -2.474 eV for **DYE 4**; -2.494 eV

for **DYE 5;** -3.149 eV for **DYE 6**; -3.204 eV for **DYE 7** and -2.514 eV for **DYE 8**. The estimated LUMO level of the standard **N719** dye is -3.43 eV (Solaronix, 2013), which is the least LUMO level followed by -3.204 eV LUMO level of **DYE 7** and-3.149 eV for **DYE 6** . The **DYE 4** has the highest LUMO energy level of -2.474 eV. The difference in the LUMO and the HOMO which indicates the electrochemical band gap of the standard **N719** dye is 1.909 eV (Solaronix, 2013), which is the least followed by 1.97ev band gap energy for **DYE 1**. This is an indications that **DYE 1** has a reduced band gap which will better serve as a sensitizer in DCCS. The electrochemical band gap of **DYE 6** and **DYE 7** were 2.281 eV and 2.81 eV which is closer to that of band gap of the standard **N719** dye. The electrochemical band of **DYE 6** and **DYE 7** will serve as better sensitizers due to their reduced values.

A summary of the absorption, emission and electrochemical properties of **DYE 1**, **DYE 2**, and the standard **N719** dye are shown in **Table 4.3** below.

Table 4.3: The absorption, emission and electrochemical properties of the dyes1, 2, 3, 4, 5, 6, 7 and 8 and the standard N719 dye.

Compound	Absorption and emission spectroscopy			Cyclic voltammetry		
	λmax (nm)	λonset (nm)	Eg (eV)	Oxidation onset(Eox-V)	HOMO Level(eV)	LUMO Level(eV)
DYE 1,	291, 355.5, 518	630	1.969	0.28	-5.08	-3.11
DYE 2	360, 478	540	2.29	0.30	-5.10	-2.81
DYE 3	352	430	2.886	0.6	-5.40	-2.514
DYE 4	353.5	430	2.886	0.56	-5.36	-2.474
DYE 5	355	433	2.866	0.52	-5.36	-2.494
DYE 6	480, 354	544	2.281	0.63	-5.43	-3.149
DYE 7	315, 392, 469	550	2.256	0.66	-5.46	-3.204
DYE 8	294 ,353	430	2.886	0.60	-5.40	-2.514
N719 DYE	314, 397, 535	650	1.909	0.54	-5.34	-3.430

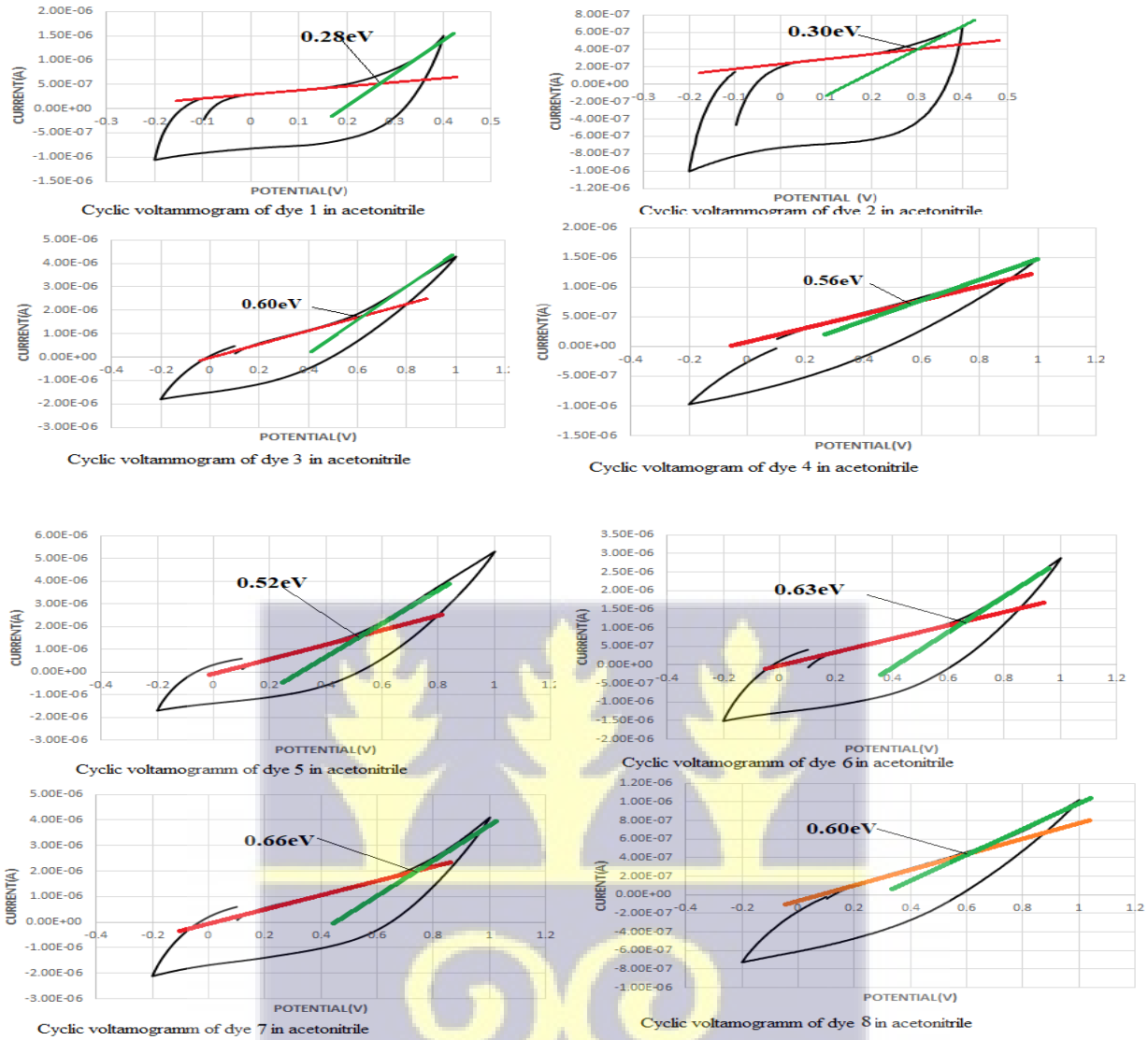

Figure 4.31 Voltamograms of Dye 1,2,3,4,5,6,7 and 8 showing the Oxidation onset

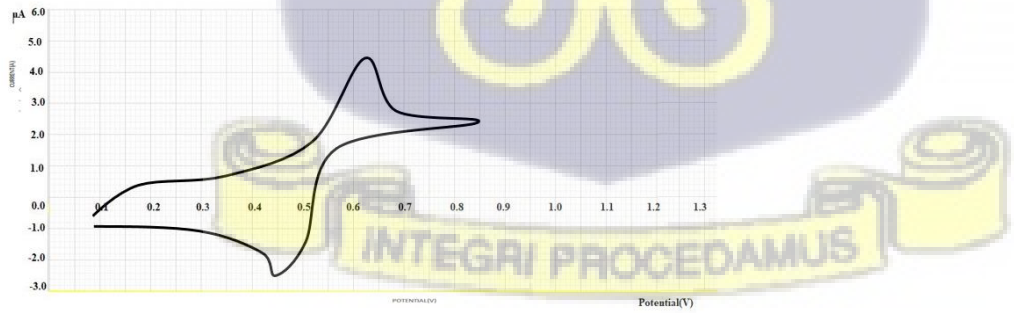

Figure 4.32 Voltamogram of ferrocene in acetonitrile

CHAPTER FIVE

5.1 Conclusion

The synthesized and purified azo dyes were characterized by the following instruments; stuart Melting Point Apparatus was used in determine the melting point, UV-Vis Spectroscopy was used to determine the chromophoric regions in azo dyes responsible for absorption, FTIR Spectroscopy was used to determine the functional groups. The ^{1}H NMR and ^{13}C NMR was used to determine the arrangement of the hydrogen and carbon atoms in the dyes and a Cyclic voltammetry was used to determine its possible ability as a sensitizer in DSSCs. The chemical structures of **DYE 1, DYE 2, DYE 3**, **DYE 4, DYE 5, DYE 6, DYE 7** and **DYE 8** were successfully elucidated.

The photochemical optical band gap **(Eg)** of the azo dyes ranged from 1.969 – 3.027 eV. The dye sensitizers showed an electrochemical oxidation onset between 0.28 -0.66 eV with **dye 1** and **dye 8** offering the most efficient potential difference to remove an electron from it molecular orbital. This can be attributed to the intense absorption that occurs in the visible region from 355.5 nm to 518 nm for the Dye 1 and 315 nm to 469 nm for Dye 2. There was better electron charge transfer between dye 1 and the TiO_2 surface.

The **Dye 1, Dye 7 and Dye 8** showed energy LUMO values that were low and close to the N719 dye. **Dye 1, Dye 7 and Dye 8** had a broader absorption in the visible region than the remaining dyes and was expected to produce the best performing device if used as solar cell sensitizer. This could be attributed to several factors including high conjugation in the pi-system, which leads to high electron distribution availability. It is estimated that, these azodyes would couple with TiO_2 surface and absorb photons from the visible light for excitation generation, as well as provide a flow of LUMO energy level for efficient charge transport and device performances.

The Dye 2, 4, 5, 6, 7 and 8 gave high LUMO energy levels compared to the standard dye. This is attributed to the poor absorption in the UV region allowing only a small fraction of visible photons to be absorbed. According to the finding of this work, synthetic azo dyes are good sensitizers for

DSSCs because of their low-cost production, easy-to-manufacture process and the narrow energy range of the HOMO-LUMO energy gap.

5.2 Recommendation

The drive to produce DSSCs that have high efficiency performance is now of great importance to the world. Research has showed that most synthetic pigments have moderate absorptions in the visible region, allowing the harvest of a fraction of sunlight and consequently raising device performance. In this regard, it is recommended that synthetic derivatives of aniline azo dyes which produced very high performing device in DSSC can be synthesized by introducing conjugated substituents (preferably aromatic or aliphatic groups) to broaden its absorption range to incorporate light (photons) in the near-infrared regions. It is also recommended that auxochrome groups or anchoring groups like $-SO_3H$, –OH, NO_2 and –COOH, be introduced on the structure of the azo dyes. The presence of these functional groups makes the molecule very soluble and environmentally friendly. The functional groups also enhance anchorage to the semiconductor surface and for efficient electron charge transfer in the DSSCs.

REFERENCES

Andualem A. & Demiss S. (2018). Review on Dye-Sensitized Solar Cells (DSSCs). *Applied Science Technology Journal*, *2*(1), 145-150

Antwi, B., Taylor R., Cameron J., Owoare R., Kingsford-Adaboh R. & Skabara P. (2016). Acceptor-Donor-Acceptor small molecules based on derivatives of 3,4 ethylenedioxythiophene for solution processed organic solar cells. *Royal Society of Chemistry Advances*. *6*(1), 1-19. https://doi.org/10.1039/C6RA22897F

Aziz, S.B., Hassan, A.Q., Mohammed, S.J., Karim, W.O., Kadir, M.F. Z., Tajuddin, H.A. & Chan, N.N.M.Y., (2019). Structural and optical characteristics of pva:C-dot composites: Tuning the absorption of ultra violet (UV) region. *Nanomaterials*, *9*(2), 216. https://doi.org/ 10.3390/nano9020216.

Banin U., Waiskopf N., Hammarström L., Boschloo G., Freitag M., Johansson E. M. J., Sá J., Tian H, Johnston M B, Herz L M, Milot R L, Kanatzidis M G, Ke W, Spanopoulos I, Kohlstedt K L.,Schatz G. C., Lewis N., Meyer T., Nozik A. J., Beard M. C., Armstrong F., Megarity C. F., Schmuttenmaer C. A., Batista V. S. and Brudvig G. W. (2021). Nanotechnology for catalysis and solar energy conversion, *Nanotechnology*, 32(1), 1-29

Bansal P., Singh D. & Sud D. (2010). Photocatalytic degradation of azo dye in aqueous TiO_2 suspension Reaction pathway and identification of intermediates products

by LC/MS. *Separation and Purification Technology Journal*, *72*(3), 357-365

Bard A. J. & Faulkner L. R (2000). *Electrochemical Methods: Fundamentals and Applications*, 2nd Edition. Wiley, New Jersey, US

Bhatia S.C. (2014). 5-Solar photovoltaic systems. *Advanced Renewable Energy Systems*, 1, 144-157.

Burrow P., Padmaperuma, A., Sapochak, L., Djurovich, P. & Thompson, E. (2006). Highly efficient blue organic light-emitting diode with an oligomeric host having high triplet-energy and high electron mobility. *Applied Physic Letters.*, *88*(1), 183503.

Carey, F & Sundberg, R. (2001). *Advanced Organic Chemistry. Part B: Reactions and Synthesis*. Fourth Edition. Molecules, New York, US

Central Intelligence Agency (2018). The CIA World Factbook, USA

Chang H, Kao MJ, Chen TL, Chen CH, Cho KC, Lai XR (2013) Characterization of Natural Dye Extracted from Wormwood and Purple Cabbage for Dye-Sensitized Solar Cells. J Photoenergy Article ID 159502:8

Ellison, D., Morris, C.E., Locatelli, B., Sheil, D., Cohen, J., Murdiyarso, D., Gutierrez, V.,Noordwijk, M. van, Creed, I.F., Pokorny, J., Gaveau, D., Spracklen, D.V., Tobella, A.B., Ilstedt, U., Teuling, A.J., Gebrehiwot, S.G., Sands, D.C., Muys, B., Verbist, B., Springgay, E., Sugandi, Y., Sullivan, C.A. (2017). Trees, forests

and water: Cool insights for a hot world. Global. *Environmental Change Journal*, *43*(1), 51–61

European Network of Transmission System Operators, ENTSO-E (2015). The Vision issued in June 2015, Brussel, Belgium

Filarowski (2010). Perkin's Mauve: The History of the Chemistry. *Resonance*, 15(9), 850-855

Gangishetty MK, Lee KE, Scott RWJ, Kelly TL (2013) Plasmonic Enhancement of Dye Sensitized Solar Cells in the Red-to-near-Infrared Region using Triangular Core–Shell Ag@SiO2 Nanoparticles. ACS Appl Mater Interfaces 5:11044–11051.

Giovannetti, R. (2012). The use of Spectrophotometry UV-Vis for the Study of Porphyrins. *Micro to Nano* Spectroscopy, 87(1), 120-124.

Grätzel M, & Moser J. E. (2001). Solar Energy Conversion, Electron Transfer in chemistry (Ed.: V. Balzani), *Energy and the Environment*,,*5*(1), 589–644

Gratzel M., Nazeeruddin K. & Baranoff E., (2011). Dye-sensitized solar cells: A brief overview. *Sol Energy*, 85(1), 1172–1178.

Grisafe K. Ni, B., W. Chakraborty, Saha A. K., Dutta S., Jerry M.,. Smith J. A, Gupta S., & Datta S.(2018). *IEEE, International Electron Devices Meeting (IEDM),1*(2),1611–1614.

Halabieh H. E., Ozzy M. & Barrett C. J. (2004). Using light to control physical properties of polymers and surfaces with azobenzene chromophores. Chemistry, *Journal of chemistry, 76*(7-8), 1445-1465.

Halls, J. J. M. & Friend R. H. (2001). *Organic Photovoltaic Devices. Clean electricity from photovoltaics: Series on photoconversion of solar energy*. M. D. a. H. Archer, R. London, Imperial College Press, Royal Holloway, University of London, UK.

Harborne, J. B., & Mabry, T. J. (2013). *The flavonoids: Advances in research*. John Wiley and Sons, Springer

Hossain MA, Park J, Yoo D, Baek YK, Kim Y, Kim SH, Lee D (2016) Surface Plasmonic Effects on Dye-Sensitized Solar Cells by SiO2-Encapsulated Ag Nanoparticles. Curr Appl Phys 16:397–403

Ihara M, Kanno M, Inoue S (2010) Photoabsorption-Enhanced Dye Sensitized Solar Cell by Using Localized Surface Plasmon of Silver Nanoparticles Modified with Polymer. Phys E Low Dimens Syst Nanostruct 42:2867–2871

International energy agency, IEA (2016). Electricity Market Report December 2016 Electricity Market Report December 2016, Paris, France.

International energy agency, IEA (2020). Electricity Market Report December 2020 Electricity Market Report December 2020, Paris, France.

International Energy Outlook, IEO (2016). U.S. Energy Information Administration, May 2016, USA

International Hydropower Association, IHA. (2015). *Ghana: assessing the sustainability of new hydropower sites*. (A. Khalil, Producer) Retrieved August 4, 2017, from International Hydropower Association: https://www.hydropower.org/blog/ghana-assessing-the-sustainability-of-newhydropower-sites

International Renewable Energy Agency, IRENA (2018). IRENA Planning and prospects for renewable power: *West Africa, International Renewable Energy Agency*, Abu Dhabi

Islam A., Sugihara H., Hara K., Singh L. P., Katoh R., Yanagida M., Takahashi Y., Murata S., Arakawa H. & Fujihashi G.(2001). *Inorganic. Chemistry,* 40(1), 5371-5380

Jakubowski L. A. (2010). Early history of the physics and chemistry of semiconductors, *Journal of Telecommunitio. and Information Technology*, *1*, 3-9

Jiang Y, Li L, Yang Y, Fan R, Y et al (2014) A simple modification of near-infrared photon-to-

electron response with fluorescence resonance energy transfer for dye-sensitized solar cells. J Power Sources 264:254–261.

Jun HK, Careemb MA, Arof AK (2016) Plasmonic effects of quantum size gold nanoparticles on dye-sensitized solar cell. Materials Today: Proceedings 3S:S73–S79

Kaung P., Sanda M., Khin & Mu S. (2014). Dye-Sensitized Solar Cells (DSSCs). *Journal of Myan Academy of Arts and Science, 12*(2),6-9

Keeley G. P. & Lyons M. E. (2009). "The effects of thin layer diffusion at glassy carbon electrodes modified with porous films of single-walled carbon nanotubes," .*International. Journal of Electrochemical. Science. 4*(1), 794–809.

Keeley G. P. & Lyons M. E. G. (2009). The effects of thin layer diffusion at glassy carbon electrodes modified with porous films of single-walled carbon nanotubes. *International Journal of. Electrochemistry Science*, 4(1), 794-809

Kumar S., Kumar V., Malyan S., Sharma J., Mathimani T., Maskarenj M., Ghosh P., & Pugazhendhi A.(2019). "Microbial fuel cells (MFCs) for bioelectrochemical Treatment of different wastewater streams", *Journal of Applied Mechanics and Fuel* 254(1), 115-526.

Kumar R., Mahiya K & Mathur D. (2011). 'Synthesis, spectral and structural characterization of Cu(II) complexes of a tridentate NNO donor Schiff base

carrying a pendant benzimidazolyl arm". *Industrial Journal of Chemistry, 50*(1), 775-780

Kunkely, H., Vogler, A.(2001), Inorganic. *Chemistry Communication Journal*, 4, 692

Lin Y-J, Chen JW, Hsiao PT, Tung YL, Chang CC, Chen CM (2017) Efficiency improvement of dye-sensitized solar cells by in situ fluorescence resonance energy transfer. J Mater Chem A 5:9081–9089

Lindsay R. J.(1979). *In Comprehensitive Organiquc*, S. D. Barton, W. D. Ollis and I. O. Sutherland, Editions, Pergamon Press: Oxford. 2, 154

Mahmood, A (2016). *Triphenylamine based dyes for dye sensitized solar cells*: a review. Solar Energy, 123,127–144

Mallikarjuna N.M., & J. Keshavayya (2020). Synthesis, spectroscopic characterization and pharmacological studies on novel sulfamethaxazole based azo dyes *Journal of King Saud University – Science Department of PG Studies and Research in Chemistry*, 1, 377-451.

Margulis GY, Lim B, Hardin BE, Unger EL, Yum JH, Feckl JM, Fattakhova-Rohlfing D, Bein T et al (2013) Highly soluble energy relay dyes for dye-sensitized solar cells. Phys Chem Chem Phys 15:11306–11312

Mchale M. (2008). “Multi step synthesis: Preparation of organic dyes”, Connexions.

Meth-Cohn, O. & Travis, A. S, (1995). The Mauveine Mystery. *Chemistry Journal*, 31, 547–549

Nazeeruddin M. K., Pechy P. & Gratzel M. (1997). Chemistry. *Communication Journal of Chemical science, 1*(2),1705-1706

Nicholson R. S. (1965). “Theory and Application of Cyclic Voltammetry for Measurement of Electrode Reaction Kinetics.” Analytical Chemistry Journal, *37(*11), 1351–1355,

Nyarko-Kumi E. (2017). “*The Electricity Situation in Ghana: Challenges and Opportunities*.” CGD Policy Paper. Washington, DC: Center for Global Development. https://www.cgdev.org/publication/electricity-situation-ghana-challenges-and-opportunities.

Pappis, I. et al (2019). *Energy projections for African countries*. A policy document, https://op.europa.eu/publication/manifestation_identi¦er /PUB_KJNA29904ENN (2019)

Pavlovic G., Racane L., Cicak H. & Kulenovic V.T. (2009). Synthesis, Spectral Properties and Applications of Some Mordant and Disperse Mono Azo Dyes Derived from 2-amino-1, 3-benzothiazole, Dyes and Pigments. *Journal of*

Chemical Science,*1*(5), 362.

Petrova, P., Ivanov, P., Marcheva, Y., & Tomova, R. (2013). Estimation of energy levels of new Iridium cyclometalated complexes via cyclic voltammetry. *Journal of chemical science*, 1(2),1-8

Pommerehene J., Vestweber H., Guss W., Mahrt R.F, Bassler H., Prorsch M. & Daub J. (1995). Efficient two layer LEDs on a polymer blend basis. *Advanced Chemistry of Matter*, *7*(6),551–554.

Pratiwi DD, Nurosyid F, Supriyanto A, Suryana R (2017) Efficiency enhancement of dye-sensitized solar cells (DSSC) by addition of synthetic dye into natural dye (anthocyanin). IOP Conf Series: Materials Science and Engineering Article ID 012012:176

Rippon J.A & Evans D.J. (2012). *Improving the properties of natural fibres by chemical treatments Handbook of Natural Fibres Processing and Applications*. Woodhead Publishing Series in Textiles, USA.

Sameiro M., Maia H.L.S. & Goncalves T. (2001). Temporary marker for biological Letters, *Journal of Chemical Biology*, 42, 7775-7777

Sboui M, Hinda L, Bouattour S, Gruttadauria M., La Parola V, Liotta L.F., & Sami B,(2021). TiO_2/Ag_2O immobilized on cellulose paper: A new floating system for enhanced photocatalytic and antibacterial activities, *Environmental*

Research Journal, 198,111-116

Scharber M. C., Mühlbacher D., Koppe M., Denk P., Waldauf C., Heeger A. J. & Brabec C. J. *Advanced Journal in Matter*, *18*(1), 789-794.

Scotter, M. (2009). The chemistry and analysis of annatto food colouring: a review. *Food Additives and Contaminants*, 26(8), 1123-1145

Sharma D, Meshra R & Raj B. (2021). Design and Analysis of Various Solar Cell Technologies for Improvements in E¨ciencies: A Review, *Research Square*,1, 1-22

Shockley W. & Queisser H. J, (1961). Photon analysis, *Journal of Applied. Physics*, *32*(1), 510-519

Silverstein, R.M., Bassler, G.C & Morrill, T.C.(1981). *Spectrometric identification of organic Compounds*" 4th edition. Wiley, New York, p. 323.

Singh, R. P., Singh, P. K., and Singh, R. L. (2014). Bacterial decolorization of textile azo dye acid orange by *Staphylococcus hominis*. *Toxicology. International Journal*, *21*, 160–166. https://doi: 10.4103/0971-6580.139797

Smil, V. (2017). Energy and Civilization: A History. Cambridge, MA: MIT Press, 568

Solarnix(2013). https://www.solaronix.com/news/the-solaronix-catalog-2013-is-out-with-

a-load-of-new-products/

Suyitno,A , Rachmad1 D. N, Zainal Arifin,B, Saputra T. J. , Omid M. A & Mirza Y. (2015). Effect of Natural and Synthetic Dyes on the Performance of Dye-Sensitized Solar Cells Based on ZnO Nanorods Semiconductor. *Journal of Applied Mechanics and Materials, 699*, 577-582

United Nations General Assembly, UNGA (2015).Transforming our world: the 2030 Agenda for Sustainable Development Resolution. A/RES/70/1, 25 1–35 (2015).

US Department of energy (2016). How does solar works? Solar energy technologies office *Post*: https://www.energy.gov/eere/solar/how-does-solar-work

Wang TH, Huang TW, Tsai YC, Chang YW, Liao CS (2015) A photoluminescent layer for improving the performance of dye-sensitized solar cells. Chem Commun 51:7253–7256

World Energy Outlook, IEA (2020). Flagship report,October, 2020

Yates, E. & Yates, A. (2016). Victorian brewer and synthetic dye chemist. *Notes and Records, 70*, 65-81

Yeats A. C., R. G. D. Taylor & P. J. Skabara,(2018) . Nanostructured Materials for Type III Photovoltaics, *The Royal Society of Chemistry*, 12, 109-153.

Zollinger H. (1994). Diazo Chemistry I: Aromatic and Heteroaromatic Compounds. By VCH Vertagsgesellschaft mbH ISBN: 3-527-29213-6., 1-2

Zollinger H. (1987). Textile Dyes: Dyeing Process and Environmental Impact Colour Chemistry.Dyes and Pigments, 92-102,ISBN-10:0471747955